# In situ mutational screening and CRISPR interference reveal that the *apterous* Early enhancer is required for developmental boundary positioning

Gustavo Aguilar[1 *] ✉, Michèle Sickmann[2 *], Dimitri Bieli[3], Gordian Born[4],

Markus Affolter[1], Martin Müller[1]✉

1. Growth and Development, Biozentrum, Spitalstrasse 41, University of Basel, Basel, Switzerland
2. Current address: Institute of Medical Virology, University of Zurich, Zurich, Switzerland
3. Current address: Mabylon AG, Wagistrasse 14, 8952 Schlieren, Switzerland
4. Current address: Arcondis, Reinach, Switzerland
5. Current Adress: Department of Biological Engineering, Massachusetts Institute of Technology, Cambridge, MA, USA

* Co-first authors

✉ Corresponding authors. Email: gusag@mit.edu, m.mueller@unibas.ch

## Abstract

The establishment of tissue axes is fundamental during embryonic development. In the Drosophila wing, the anterior/posterior (AP) and the dorsal/ventral (DV) compartment boundaries provide the basic coordinates around which the tissue develops. These boundaries arise as a result of two lineage decisions, the acquisition of posterior fate by the selector gene *engrailed* (*en)* and of dorsal fate by the selector gene *apterous* (*ap*). While the *en* expression domain is set up during embryogenesis, *ap* expression only starts during early wing development. Thus, the correct establishment of *ap* expression pattern with respect to *en* must be tightly controlled. Here we have functionally investigated the transcriptional inputs integrated by the "early" *ap* enhancer (apE) and their requirement for correct boundary formation. Detailed mutational analyses using CRISPR/Cas revealed a role of apE in positioning the DV boundary with respect to the AP boundary, with apE mutants often displaying mirror-image anterior wing duplications. We then designed and applied methods to accomplished tissue-specific enhancer disruption via dCas9 expression. This approach allowed us to dissect the spatio-temporal requirement of apE function, challenging the mechanism by which apE miss-regulation leads to AP defects. Base-pair resolution analyses of apE uncovered a single HOX binding site essential for wing development, which, when mutated, led to wingless flies. In the course of our studies, we found that the HOX gene Antennapedia (Antp) is fundamental for *ap* expression. In addition, we demonstrated that the transcription factors Pointed (Pnt), Homothorax (Hth) and Grain (Grn) are necessary for apE function. Together, our results provide a comprehensive molecular basis of early *ap* activation and the developmental consequences of its miss-regulation, shedding light on how compartmental boundaries are set up during development.

## Keywords

Enhancer, CRISPR, HOX, Antennapedia, *apterous*, wing disc, dCas, dCRISPR, GATA

## Introduction

During development, cells segregate into different populations, often in a lineage-restricted manner. Between these populations, developmental boundaries arise as essential organizing centers, providing the mechanical and chemical cues required for tissue patterning and growth (Irvine & Rauskolb, 2001). The Drosophila imaginal wing disc has served as a discovery platform for the study of developmental boundaries (Tripathi & Irvine, 2022). This tissue is subdivided by two lineage decisions. During embryogenesis, roughly half the cells of the future wing disc express the selector gene *engrailed* (*en*) (Morata & Lawrence, 1975). *en* expressing cells will acquire posterior (P) fate, while cells without *en* will adopt anterior (A) fate. These two populations will thereafter be segregated via the establishment of the Antero-Posterior (AP) compartment boundary (Garcia-Bellido et al., 1973, 1976). The AP boundary is essential for medio-lateral patterning of the wing, via the action of the morphogens Hedgehog (Hh) and Decapentaplegic (Dpp) (Basler & Struhl, 1994; Capdevila & Guerrero, 1994). The second lineage subdivision occurs during early wing disc development, when the gene *apterous* (*ap*) starts to be transcribed in a population of cells of the proximal wing disc (Cohen et al., 1992). *ap* encodes a LIM-type homeodomain transcription factor that is responsible for instructing dorsal (D) identity, together with its cofactor CHIP (Blair et al., 1994; Diaz-Benjumea & Cohen, 1993; Fernández-Fúnez et al., 1998; Garcia-Bellido et al., 1976; Milán & Cohen, 1999; van Meyel et al., 1999). Cells lacking *ap* expression will become ventral (V). The DV boundary instructs proximo-distal patterning via the morphogen Wingless (Wg) (Couso et al., 1993; Neumann & Cohen, 1997; Zecca et al., 1996). At the boundary intersection, the secreted signaling molecules expressed at the DV (Wg) and the AP (Dpp) boundaries synergistically promote specification and growth of the wing pouch, the larval precursor of the wing blade (Couso et al., 1995; Kim et al., 1997; Williams et al., 1994). The two boundaries thereby provide the coordinate system according to which the four segregated quadrants of the developing wing (anterior-dorsal, AD; anterior-ventral, AV; posterior-dorsal, PD; and posterior-ventral, PV) develop.

The downstream effectors of *ap* during wing development are well characterized (Blair et al., 1994; Klein et al., 1998). However, little is known about how the expression pattern of *ap* is set up with respect to that of *en.* In other words, how is the DV boundary positioned with respect to the AP boundary?

Interestingly, $ap^{blot}$, a mutation within the *ap* cis-regulatory landscape, has been shown to produce mirror image transformations of the P compartment into the A compartment (Whittle, 1979). How such interaction between *ap* and the AP specification program arises is unknown. Previously, we have found that $ap^{blot}$ maps to the *ap* Early enhancer (apE), the regulatory module responsible for *ap* early transcription (Bieli, Kanca, Gohl, et al., 2015; Bieli, Kanca, Requena, et al., 2015). In later stages, *ap* positively regulates itself via the enhancer apDV, at least in the wing pouch (Figure 1 – figure supplement 1, (Bieli, Kanca, Requena, et al., 2015)). This regulatory feedback is likely to maintain the expression pattern established earlier by apE. The main upstream factor known to regulate apE is the EGFR pathway. EGFR signaling has been shown to be both required and sufficient for *ap* transcription (Wang et al., 2000; Zecca & Struhl, 2002).

In this study, we have taken a bottom-up approach, from the sequence of the enhancer to the development of the tissue. We have genetically dissected apE using CRISPR gene editing and found that apE is required for correct DV positioning. apE hypomorphic mutants displayed problems in the growth of the posterior-dorsal compartment and subsequent mirror image duplications of the A compartment. The EGFR core transcription factor (TF) Pointed (Pnt) and the TF Homothorax (Hth) are responsible for early *ap* expression via apE. The loss of these factors in the posterior compartment resulted in mirror image duplications of the wing. Base pair-resolution mutation analyses of apE subregions uncovered a HOX-GATA complex fundamental for wing formation, of which we identify Grain (Grn) as the GATA TF and propose

Antennapedia (Antp) as the HOX. Finally, in order to dissect the spatio-temporal requirement of apE, we have implemented a novel methodology for enhancer inactivation, solely based on the recruitment of catalytic-dead Cas9 (dCas9) to the enhancer. Using this tool, we validated the results of our mutational analyses and dissected the spatial requirement of apE function.

## Results

### Precise manipulation of endogenous apE enhancer

The 27 Kb intergenic spacer upstream of the *ap* transcription start site (TSS) contains five conserved regions, named C1 to C5 (Bieli, Kanca, Requena, et al., 2015). We have previously replaced this entire intergenic sequence by an *attP* site, thereby generating a "landing site" in the locus. Subsequently, different attP-containing fragments were re-integrated via φ C31-mediated transgenesis. This approach revealed three distinct modules required during wing development: the apE enhancer, within C2, required for early *ap* expression; the DV enhancer, within C5, responsible for robust *ap* expression along the DV boundary; and a Polycomb response element (PRE), immediately upstream to the TSS, required for maintenance of the transcriptional state of *ap* (Bieli, Kanca, Requena, et al., 2015). While useful to study the overall cis-regulatory architecture, reintegration into this landing site resulted in changes in the relative distance of these individual regulatory modules with respect to the TSS and entailed large genomic deletions. In order to study apE in its endogenous context, we decided to construct a new landing site.

The minimal enhancer region contained in apE encompasses 463 bp in the proximal area of C2, hereafter named OR463 (Figure 1 – figure supplement 2). We have previously shown that reintegration of OR463 alone is sufficient to rescue the wing phenotype produced by the loss of C2 (Bieli, Kanca, Requena, et al., 2015). Based on these results, we decided to substitute OR463 by an *attP* site using CRISPR/Cas9 editing (Figure 1 – figure supplement 3 and Materials and Methods). We have also demonstrated that crosstalk between apE and *dad* enhancers is responsible for the dominant *Xasta* (*Xa*) phenotype (Bieli, Kanca, Gohl, et al., 2015). Thus, in order to positively select for CRISPR/Cas9-mediated HDR, the Dad13 enhancer was inserted, flanked by FRTs, alongside the *attP* site (Figure 1 – figure supplement 3A, B). As predicted, heterozygous insertion events of the *attP* coupled to Dad13 were easily identified by their characteristic wing phenotypes (Figure 1 – figure supplement 3A'). Flippase was subsequently used to excise Dad13 (Figure 1 – figure supplement 3B). The resulting substitution of OR463 by the *attP* site resulted in fully penetrant loss of wings in homozygosis (Figure 1F, Figure 1 – figure supplement 3B'). The *attP* site was then used to re-integrate the different OR463 fragments via φC31-mediated insertion, along with the *mini-yellow* marker, which was later removed using the FRT/Flippase system (Figure 1 – figure supplement 3C, D).

Reintegration of OR463 sequence into this landing site resulted in 100% of normal wings in homozygosis (Figure 1 – figure supplement 3D') and 95% normal wings when in a hemizygous background (over the $ap^{DG3}$ deletion, which encompasses the whole intergenic spacer (Bieli, Kanca, Requena, et al., 2015)). This approach was used to generate all the apE mutants described in this study.

### OR463 contains two highly conserved domains required for wing development

Bioinformatic analysis of OR463 uncovered four main modules based on sequence conservation among related insects (Figure 1A, Material and methods). We further refined those modules by analyzing the conservation of TF binding sites using MotEvo (Arnold et al., 2011). This analysis permitted us to subdivide

OR463 into four regions of high conservation (m1 to m4) and six less well-conserved inter-regions (N1 to N6) (Figure 1B).

To evaluate the functional requirement of each region, we generated fly strains bearing precise deletions of each of them. Homozygous and hemizygous animals of all the mutants reached adulthood, displaying altered mutant phenotypes only within the wings and halteres. Scoring of wing phenotypes uncovered two genomic regions which, when deleted, resulted in higher penetrance of mutant phenotypes (Figure 1C). The first area was centered in m3, whose deletion resulted in fully penetrant loss of wings (Figure 1G). Deletion of the neighboring region N4 also yielded a very high number of defective wings. The second sensitive area was located around conserved region m1 (N1, m1, N2), with both *Δm1* and *ΔN2* deletions yielding similarly penetrant phenotypes. The penetrance of the phenotypes was exacerbated when the aforementioned mutant alleles were scored in hemizygous background (over $ap^{DG3}$) (Figure 2D).

Excluding the *Δm3* deletion, the other mutants displayed similar phenotypes, although varying in quantity and quality. Interestingly, many of these wings presented a posterior compartment outgrowth, in which the vein pattern was reminiscent to that of the anterior wing, and anterior margin bristles were found in its posterior edge (Figure 1H). In those wings, the anterior compartment was largely unaffected.

In some of the most penetrant alleles, and especially when the mutants where in hemizygosis, wings did not present an outgrowth, but rather partial mirror image transformations of the margin bristles of the P compartment into A compartment identity, accompanied by unusual vein trajectories in the P compartment (Figure 1I). This wing phenotype was often associated with a reduction in P compartment size. In some of these cases, the P compartment was hardly detectable, and the overall wing size was severely reduced, resulting in roundish wings in which only A and tip margin bristles were present (Figure 1I'). Some of these phenotypes are reminiscent of those reported for $ap^{Blot}$ (Whittle, 1979) and point towards a yet undescribed crosstalk between *ap* early expression and the AP specification program.

### OR463 disruption results in misplacement of the DV boundary with respect to the AP boundary

In order to dissect how these mirror image duplications arise, we analyzed the expression pattern of Ap in third-larval stage (L3) wing imaginal discs. In control discs (wild-type OR463 reintegrated into the landing site), the Ap expression domain (Figure 2A) mimicked that seen in wild-type discs (Bieli, Kanca, Requena, et al., 2015). Wg was detected in its characteristic stripe along the DV boundary and in the two concentric rings of the hinge (Figure 2A). In Δ*m1* homozygous mutants, disruption of the Ap expression pattern was most evident in the P compartment, where the DV boundary was curved towards the hinge (Figure 2A'). This deformation of the DV boundary was also revealed by Wg immunostaining (Figure 2A'). In these cases, Wg expression in the P hinge also seemed altered. The deformation of DV compartmentalization was also observed in other alleles carrying deletions within the OR463 region, as shown by anti-Ap immunostaing (Figure 2 – figure supplement 1). As described for adult wings, the severity of the wing disc phenotypes was exacerbated in hemizygous background, with wing discs that presented a more obvious deformation of Ap pattern in the P side of the wing and overall reduced size (Figure 2A''). In all cases, intensity of anti-Ap staining was comparable among the wild-type and the different mutants, suggesting a role of apE in setting up the proper *ap* expression domain rather than its expression level.

P to A mirror image duplication of the wing has been described upon different genetic perturbations (Baonza et al., 2000; Brower, 1984; Guillén et al., 1995; Hidalgo, 1998; Recasens-Alvarez et al., 2017; Uemura et al., 1993). A paradigmatic case is the loss of *en* expression. *en* mutant clones in the P compartment lead to loss of P identity and the formation of a new AP boundary around the clone (Brower, 1984; Tabata et al.,

1995). Thus, we analyzed En expression in wing discs of *Δap$^{E}$* hemizygous mutants (Figure 2 – figure supplement 2). While wing disc size is severely affected compared to control, En localization, as revealed by immunostaining, presented little change in its expression pattern. To account for the possibility that *en* expression would be lost in some cells during development, thereby leading to the duplications, we analyzed the lineage of *en* positive cells in both control and Δ*m1* hemizygous background. To that end, we made use of gTRACE (Evans et al., 2009), a genetic tool that uses the expression of a Gal4 line of interest to both immortalize a fluorescent reporter (via Flp mediated excision of a FRT cassette, leading to the constitutive expression of a *tub*-GFP reporter) and at the same time reveal current Gal4 levels (via an *UAS*-RFP transgene). In both control and Δ*m1* hemizygous background, *en*-Gal4 revealed highly overlapping patterns of lineage and current expression (Figure 2 – figure supplement 2B, C). Thus, these experiments discard the loss of *en* expression as a driver for the duplications observed in *ap* mutants. In addition, the experiment revealed that in Δ*m1* mutants, the P compartment is severely reduced and that the position of the AP boundary along the pouch was also distorted (Figure 2 – figure supplement 2C).

Motivated by this finding, we measured the relative size of the P wing disc compartment in several of the OR463 mutants, revealing a reduction in all of them (Figure 2B), in agreement with the results of the gTRACE experiment and the phenotypes of adult wings (Figure 1G). The relative position of the DV and AP boundaries was then studied by co-immunostaining of Ap and Ptc proteins. In control discs, DV and AP boundaries form perpendicular axes, with a single intersection in the middle of the wing pouch, dividing the disc in four quadrants (DA, DP, VA and VP; see Figure 2C). In Δ*m1* hemizygous discs, PD quadrant size was strongly reduced (Figure 2C',). This resulted in two intersection points and long stretches where both the DV and the AP coincide. In cases where the size of PD was less compromised, as in Δ*N1* hemizygous mutants (Figure 2C''), these two intersections were located further apart. Quantification of PD quadrant size revealed a great decrease of relative area in different OR463 mutants (Figure 2B').

To identify the nature of the posterior outgrowths, we performed anti-Vestigal (Vg) antibody staining of *Δm1* mutants (Figure 2 – figure supplement 3A). Vg is a key regulator of wing specifications and also participates in wing growth and patterning (Baena-Lopez & García-Bellido, 2006; Kim et al., 1996; Zecca & Struhl, 2007a). In those discs, in which the stripe was extended and the P compartment was enlarged, Vg was detected throughout the outgrowth, supporting the wing pouch identity of this region (Figure 2 – figure supplement 3B). Hemizygous *Δm3* mutants presented a highly reduced anti-Vg signal, which suggests that no wing pouch is specified in these mutants (Figure 2 – figure supplement 3C).

### A model to explain the adult patterning defects of OR463 mutants

Intersection of the AP and DV boundaries is crucial for wing specification, patterning and growth via Dpp and Wg signals. Wild-type wings present a single intersection of the AP and DV boundaries, around which the four wing quadrants (DA, DP, VA and VP) grow coordinately. During morphogenesis, the disc evaginates along the DV boundary to form the adult wing (Aldaz et al., 2010; Fristrom & Fristrom, 1975) (Figure 2D, Figure 2 – figure supplement 4A). Our results indicate that OR463 is fundamental for setting up the *ap* expression pattern, and that the P compartment is the most sensitive to its mutation. Thus, we tried to explain the diversity of adult phenotypes, considering changes in the *ap* expression domain within the P compartment. We hypothesized that the number of intersections of DV and AP boundaries as well as the distance between them could explain the distinct adult phenotypes observed in the different OR463 mutants.

1. In the cases when PD is very small or absent, no outgrowth would be observed, as there is only one intersection point, or two intersections that are very close to each other. In these cases, both AP and

DV boundaries will largely coincide (Figure 2D' and Figure 2 – figure supplement 4C). Upon eversion, the PV compartment will be opposed by issue with AD identity, thus resulting in partial transformation of the margin and venation patterns into A identity. This is in accordance with the results presented in Figure 1, where most of the adult wings analyzed presented only partial transformation of the wing margin. Also, it explains why the venation pattern is often disrupted, since during apposition, dorsal and ventral epithelia will present different venation patterns.

2. When the size of PD is affected but still occupies a significant area (as in N1/DG3 animals, see Figure 2C), the wing disc presents two intersections that are located far from each other. In these cases, two wing pouches would be specified and an outgrowth would be formed (Figure 2D'', Figure 2 – figure supplement 4B). In the wing margin of this outgrowth, both AP and DV boundaries coincides. We predict that the D side will present A fate in this outgrowth, while the V side will have P fate, causing only A mirror-image duplication of the D side.

3. Finally, in the cases in which *ap* expression is depleted from P and affected in the A compartment, AP and DV boundaries do not intersect. However, if the boundaries are close enough, they would induce slight wing pouch growth (Figure 2 – figure supplement 4D). In these wing discs, the DV boundary will be fully embedded in the A compartment, and thus, all the wing margin will present A identity. Indeed, the wings showing the most drastic size defects among the different OR463 mutants only presented A and tip margin (Figure 1l').

   This model predicts that in both the P outgrowths (Figure 2 – figure supplement 4B) and the P to A mirror-image duplications (Figure 2 – figure supplement 4C), the D compartment presents AD identity. Consistent with our model, we could identify campaniform sensillae in Δ*m1* homozygous mutant wings (Figure 2 – figure supplement 4E) as well as in other OR463 mutants (data not shown); these sensillae are specialized sensory organ only present in the AD compartment of the wing blade (Dinges et al., 2021).

### The posterior hinge is severely affected in OR463 mutants

The wing pouch grows surrounded by (and at the expense of (Zecca & Struhl, 2007b)) the presumptive wing hinge. The hinge does not have a passive role in wing disc growth but also provides growth factors required for cell division. In particular, JAK/STAT ligands (Unpaired 1-3) derived from the hinge have been found to promote posterior growth (Recasens-Alvarez et al., 2017). Loss of JAK/STAT signaling in P cells results in mirror image duplications that highly resemble those seen in OR463 mutants. *ap* expression is indispensable for hinge development (Metz, 1914). Indeed, apE mutants totally lack this structure (Bieli, Kanca, Requena, et al., 2015). Thus, we analyzed the morphology of the hinge in OR463 mutants. We labeled the hinge by immunodetection of the hinge-specific TF Homothorax (Hth). Compared to control discs, in which the P proximal hinge is present (Figure 2 – figure supplement 5A), hemizygous Δ*m1* mutants completely lacked this region (Figure 2 – figure supplement 5A').

We then assessed the expression of the JAK/STAT ligand Unpaired 1 (Upd1). *upd-1* is expressed in five areas in third instar wing imaginal discs, in three main spots in the dorsal hinge and in two weaker regions in the ventral body wall (Johnstone et al., 2013). This pattern was faithfully captured via a *upd*-Gal4 line driving the expression of *UAS*-CD8:GFP (Figure 2 – figure supplement 5B). As expected, given the strong hinge phenotypes of OR463 mutants, *upd*-Gal4>*UAS*-CD8:GFP did not display any P signal in the proximal area of the wing when OR463 was deleted (Figure 2 – figure supplement 5B').

These results demonstrate that the main P source of JAK/STAT signaling in the disc is absent in OR463

mutants, suggesting that the similar phenotypes produced by defective JAK/STAT signaling and by mutations in OR463 might be related.

### Spatio-temporal analysis of apE via dCas9

The functional dissection of regulatory regions has classically relied on the generation of mutants. Such mutant analyses, however, do not offer any spatio-temporal information of enhancer function. Instead, reporters are normally employed as indirect readouts. Recently, expression of catalytically-dead Cas9 (dCas9) has been proposed as a means to inhibit TF-DNA binding in cell culture (Shariati et al., 2019) in a CRIPR interference (CRISPRi) setup (Qi et al., 2013). Given the high sensitivity of OR463 to perturbations, we speculated that localized expression of dCas9 could result in steric hindrance, preventing the activity of the enhancer (Figure 3A). To achieve spatio-temporal control over dCas9 expression, we constructed a fly line in which dCas9 was placed under the control of *UAS* enhancer sequences. Expression of dCas9 by the posterior driver *en*-Gal4 did not result in major phenotypes at 23º or 25º degrees when combined with a control gRNA (Figure 3C, see Materials and Methods), indicating that dCas9 does not dramatically alter the cell's physiology. To target dCas9 to the OR463 locus, we generated a transgene encoding four ubiquitously expressed gRNAs (*U6*-OR463.gRNAx4). Three of these gRNAs targeted the vicinity of m3 (Figure 3B), the region that displayed the strongest phenotypes in the deletion analysis (Figure 1).

Our mutation analysis suggests that loss of OR463 activity in the P compartment is responsible for the mirror image duplications observed in OR463 mutants (Figure 2, Figure 3 – figure supplement 1). We directly tested this assumption by expressing dCas9 using *en*-Gal4 in the presence of OR463 gRNAs. This manipulation yielded wings with posterior defects (Figure 3D), highly similar to those shown in Figure 1. Interestingly, the phenotype most often detected at 23º degrees was the presence of P outgrowths (with some A bristles). Higher expression of dCas9 (at 25º degree) yielded a majority of wings in which the posterior edge was partially transformed into A identity. The wing discs obtained from these experiments (at 23º degree) revealed a reduction of PD quadrant size, with the concomitant mispositioning of the DV and AP compartmental boundaries, which intersected twice (Figure 3E and F). These experiments independently confirm the crucial role of OR463 in correctly positioning the DV boundary and demonstrate that it is the loss of apE in the posterior compartment which is driving the AP mirror-image duplications. In order to confirm the spatial specificity of enhancer inhibition, dCas9 was also expressed using *ptc*-Gal4 in the presence of OR463 gRNAs. In this case, *ap* expression domain was divided in two, with no expression along the central pouch (Figure 3G). This broad repression band coincides with the expression pattern of *ptc* in early wing discs. This result confirms that dCas9 can inhibit enhancer function with high spatial resolution *in vivo*.

To define the developmental time window during which the apE enhancer remains sensitive to repression, we combined the temperature-sensitive *tub*-Gal80$^{ts}$ system with temporally controlled expression of dCas9. Animals carrying the *en*-Gal4, *tub*-Gal80$^{ts}$, *UAS*-dCas9 and *U6*-OR463gRNA(4x) transgenes were maintained at 18 °C to suppress dCas9 expression. Independent sets of embryos were then shifted to 29 °C at successive developmental intervals ranging from 0 to 168 h after egg laying (AEL), so that dCas9 induction occurred at distinct time points in development (Figure 3H). Under these conditions, dCas9 transcription was induced only after the temperature shift, while the gRNAs were expressed constitutively. Wing phenotypes were quantified in adult progeny as a readout of apE enhancer perturbation. When dCas9 was expressed from embryonic or early larval stages (0–48 h AEL), nearly all wings (70–90%) displayed severe *ap*-like phenotypes, including posterior compartment duplication and loss of anterior–posterior boundary integrity. Shifting animals later (48–72 h AEL) still produced a majority (~66%) of abnormal wings,

whereas induction after 72 h AEL resulted in progressively weaker effects and complete loss of phenotypes by 96 h AEL (Figure 3H').

These results delineate the developmental period during which apE activity is required for proper wing patterning. Perturbation during the first half of the second larval instar (≤ 96 h at 18 °C) was sufficient to elicit strong *ap*-like transformations, consistent with the enhancer being functionally required during early larval stages and becoming dispensable thereafter. The temporal decline in phenotype penetrance thus reflects the progressive loss of apE sensitivity to dCas9-mediated repression, providing a precise estimate of when its activity is no longer required for wing morphogenesis.

## Pnt and Hth are required for m1-m4 activity

Having established the requirement of OR463 activity during wing development and boundary positioning, we analyzed TF factors responsible for its activity pattern. m1 bioinformatic analyses identified two main TF binding sites, predicted to be recognized by Hth and an TF from the E26 transformation-specific (ETS) family (Figure 4A). The m4 region was also predicted to be recognized by ETS TFs, however, its deletion had minor effect (Figure 1C). In order to accentuate the possible phenotypes caused by deletions within apE, all subsequent m1 deletions were generated in a background which lacked m4. We generated small deletions encompassing each of the putative binding sites (Figure 4A). Scoring of the phenotypic penetrance in homozygosis (Figure 4B) and hemizygosis (Figure 4B') revealed that both sites were important for wing development, the ETS binding site having the biggest effect when deleted. Analysis of DV and AP boundary position based on immunostaining revealed that deletion of the different binding sites in hemizygosis resulted in reduced size of the PD quadrant (Figure 4C). Adult wings of the different mutants resembled the loss of m1, amid a reduction in the penetrance of the phenotypes (data not shown).

We then knocked-down the expression of the TFs predicted to bind m1, Pnt and Hth, via RNAi expression in the posterior compartment using *en*-Gal4. Affected cells were labeled using *UAS*-CD8:GFP. Strikingly, when compared to control wing discs, *hth*RNAi expression resulted in drastic reduction of the PD quadrant, mimicking the loss of m1 (Figure 4D). Unfortunately, adult phenotypes could not be studied, since these animals did not reach adulthood.

We have previously demonstrated that the ETS factor Pnt is able to bind apE (Bieli, Kanca, Requena, et al., 2015), making it an ideal putative m1 input. In addition, deletion of most conserved Pnt binding sites in an apE reporter reduced its activity (Bieli, Kanca, Requena, et al., 2015). Expression of *pnt*RNAi resulted in a reduction of the PD quadrant (Figure 4D). In this case, a posterior outgrowth was formed, mimicking that of the phenotypes caused by the loss of the ETS binding site in m1. *en*Gal4>*pnt*RNAi animals reached adulthood, displaying outgrowths in the P compartment (Figure 4E), confirming previous reports (Baonza et al., 2000). As it is the case for some of the different OR463 mutants, these outgrowths presented partial P to A transformation. In addition, campaniform sensillae were identified in the transformed compartment (Figure 4E).

To address the role of these TFs in apE activation, we tested the effect of the *pnt* and *hth* knockdown on the expression of an apE-LacZ reporter fusion. apE is mainly expressed during early larval stages. Thus, we choose mid L2 wing discs for this comparison. As before, *UAS*-CD8:GFP was used to label the manipulated cells. In these early discs, both Ap staining and apE-LacZ reporter were strongly reduced upon *pnt*RNAi expression (Figure 4F). In the case of *hth*RNAi, we observed a total abrogation of both (Figure 4F). Together, these results strongly indicate that both Hth and Pnt are required for early *ap* expression via

m1.

## High-resolution m3 analysis suggests a novel HOX-GATA complex required for wing development

Our mutation analysis revealed that the most sensitive region of OR463 is m3 (Figure 1). Compared to controls, Ap expression was reduced to a small group of cells in the hinge upon *Δm3* deletion (Figure 5A). As expected from the adult phenotypes, these mutants lacked the wing pouch, with the inner ring of Wg expression reduced to a single point (Figure 5A'). Enhancer activity was then tested using apE-LacZ reporters. Despite apE-LacZ being expressed mainly during early larvae development (Bieli, Kanca, Requena, et al., 2015), LacZ is highly stable within cells, which permits, upon long exposure to X-Gal, the rough evaluation of enhancer activity in L3 wing discs (Figure 5B). Deletion of m3 in this setting dramatically reduced X-Gal staining (Figure 5B'), indicating that the factors binding m3 are indispensable for apE enhancer activity.

Bioinformatic analysis of m3 revealed two highly conserved DNA regions, recognized by putative GATA and HOX TFs. To avoid possible artifacts derived from the sequence rearrangement that deletions produce, we generated a library of fly strains bearing precise nucleotide substitutions in pairs (G→T, A→C, T→C and C→A), allowing the evaluation of the functional dependency of each base-pair within the region in the endogenous setting (Figure 5C). Phenotypic scoring revealed that the sequences associated with both the putative GATA and HOX binding sites were required for normal wing development (Figure 5D). Mutations within the GATA binding site resulted in phenotypes resembling those described for other OR463 mutants (Figure 5E'). Mutations affecting the HOX binding site were comparatively stronger and more penetrant (Figure E'''). Four of the lines carrying mutations within the predicted HOX binding site yielded no wings (Figure E''), indicating a strong requirement of this putative binding site for wing development. The same results were obtained when the binding sites were deleted individually (Figure 5 – figure supplement 1A, B). Deletion of the predicted HOX binding site resulted in the same Ap distribution as the complete deletion of m3 (Figure 5 – figure supplement 1C).

The very high conservation of the two site suggests that both factors may interact during enhancer activation. To genetically test this hypothesis, we designed a series of mutants in which we modified the distance between these binding sites. The normal spacing was either expanded to 6bp or contracted to 2bp (Figure 5 F, Figure 5 – figure supplement 2A). When spacing was increased, all wings presented defects and, in 28% of the cases, wings were totally missing (n=110) (Figure 5 – figure supplement 2B). Reduction of the spacer sequence resulted in comparatively milder phenotypes, yielding 30% of normal wings and most of the other having a posterior compartment outgrowth (n=155) (Figure 5 – figure supplement 2C). These results suggest that the distance between these transcription factors is important for the correct functioning of the enhancer, likely implicating a yet unknown GATA-HOX complex involved in wing development.

m3 bears a strong sequence identity with m2. In fact, both regions are predicted to contain one GATA and one HOX binding sites. In contrast to the 5bp separation between these sites in the m3 region, the m2 binding sites are separated by 11bp. As an independent test for the requirement of correct spacing, we evaluated whether reducing the distance of m2 binding sites could rescue the lack of m3, whose deletion results in fully penetrant loss of wings (Figure 1G, Figure 5 – figure supplement 2E). Interestingly, reducing the spacing of m2 in *Δm3* mutants reduced to 69% the loss of wings (Figure 5G. The most frequent phenotype among the remaining 31% were tube-like wings (Figure 5 – figure supplement 2F'). In rare

cases, more normal wings were observed (Figure 5 – figure supplement 2F''). This small but significant rescue further supports the hypothesis that the interaction between a GATA and a HOX factor upon DNA binding is important for OR463 activity.

### Grn is fundamental for wing development

The *Drosophila* genome contains five genes encoding GATA TFs: *pannier (pnr), grain (grn), GATAd, GATAe and serpent (srp)*. So far, only *pnr* has been involved in wing disc development (Garcia-Garcia et al., 1999); however, its expression pattern is constrained to the most proximal region (Ramain et al., 1993), with its loss of function being associated with defects in the notum. *grn* expression has been detected in the wing hinge and pouch (Brown & Castelli-Gair Hombria, 2000; Everetts et al., 2021). However, mutant clonal analysis yielded no phenotypes in this tissue (Brown & Castelli-Gair Hombria, 2000).

We knocked-down these factors via RNAi expression in the P compartment using *en*-Gal4. *UAS*-GFP was used to mark the manipulated cells. To increase knock-down efficiency, we included *UAS-dicer* in all crosses. Among the four *grn*RNAi transgenes available from Bloomington, a test experiment indicated that two of them were suitable for our purposes (the other two had no phenotypic consequences upon expression). *grn*RNAi$^{BL34014}$, when combined with *UAS-dicer; en-Gal4, UAS-GFP,* produced flies with abnormal notum and/or wings at low frequency (11%). Among the phenotypes, we observed loss of the wing or the notum and wings with anterior image duplications, as well as others displaying reduced P compartment sizes (Figure 6A). The other *grn*RNAi stock (BL27658), when expressed with the same driver line, lead to developmental arrest in white pupae. This line was used to study the effect of *grn* depletion in the wing imaginal discs. This experiment revealed a dramatic defect in P growth compared to control discs (Figure 6B). In all cases, P cells did not show any Ap expression. As a result, the P compartments did not remain associated with the DA cells, positioning them randomly within the rest of the disc. This “floating” nature of the P compartment is likely to explain the diversity of adult phenotypes observed with the *grn*RNAi$^{BL34014}$ transgene. In some cases, the P compartment was located close to the DV boundary, promoting some degree of pouch growth but leading to partial or total notum loss (Figure 6B'). In other cases, P cells ended up in the notum region, leading to somewhat proper patterning of this region but resulting in dramatic defects of the hinge and pouch (Figure 6B'').

To independently validate these results, we generated tissue-specific CRISPR knockouts of *grn*. Ubiquitously expressed *grn* gRNAs (*U6-grn*.gRNAs) were combined with *UAS*-Cas9 under the control of en-Gal4. P cells were marked using *UAS*-CD8:GFP. In these cases, the P compartment was totally depleted in mid L3 wing discs (Figure 6C), supporting the results obtained with RNAi. In order to study *ap* expression in these discs, we decided to analyze discs at an earlier timepoint (mid L2). At this time, P cells had not been lost and GFP-expressing cells still occupied a considerable area of the wing. Ap protein was not detected in P cells (Figure 6D). Expression of the apE-LacZ reporter was also abrogated (Figure 6D), suggesting that *grn* is required for *ap* transcriptional activation via apE.

*grn* expression during wing disc development was then analyzed using a *grn*$^{GFP}$ transgene that contains all the cis-regulatory information (Kudron et al., 2018). In agreement with previous reports (Brown & Castelli-Gair Hombria, 2000), Grn:GFP was detected throughout the wing disc already in very early larval stages, but mainly in the hinge, where it was enriched in the A compartment. In addition, we observed that the area with the highest Grn:GFP signal was located around the contact between the tracheal system and the disc proper (Figure 6 – figure supplement 1).

### Antennapedia is indispensable wing development and *ap* expression

Our results demonstrated that there is a single putative Homeodomain-DNA interaction in OR463 that is indispensable for wing development (Figure 5E''). However, the homeodomain-containing protein binding to this site remains to be characterized. The fly genome contain 103 genes that encode proteins with homeobox domains (Bürglin & Affolter, 2016). Among those, a plausible candidate, Antennapedia (Antp), is responsible for the embryonic identity of the segment T2, from which the wing discs derive. Supporting an instructive role in wing formation, *Antp* overexpression specifies ectopic wings in the head under certain genetic conditions (Kurata et al., 2000; Prince et al., 2008). Recent reports demonstrated that *Antp* is required during larval stages for wing disc morphogenesis and wing margin development (Paul et al., 2021). However, the wings presented in this study showed mild phenotypes compared to the total loss of wings seen in *Δm3* mutants. We thus speculated that *Antp* would play a role in the early activation of the enhancer. Such an early role of Antp in wing disc development could have been easily missed in previous studies, which only depleted *Antp* during larval stages. Supporting an early role of Antp in wing development, early *Antp* MARCM clones generated during the first 24h of development were never retrieved in larval stages in the disc proper, and only very rarely in the peripodial membrane (Figure 7 – figure supplement 1A). Interestingly, clones generated at 48h in development did not affect anti-Ap levels (Figure 7 – figure supplement 1B), indicating that *Antp* is dispensable for *ap* expression in mid-late larval stages.

To deplete *Antp* during embryonic development, tissue-specific CRISPR/Cas9 was employed. First, we designed flies expressing ubiquitously-expressed gRNAs targeting both the first protein-coding exon of *Antp* and its third protein-coding exon (which encodes the homeodomain) (Figure 7A). Second, to target the wing primordium as early as the disc is determined, we employed the driver *sna*1.7-Gal4, specifically expressed in the embryonic primordia of the wing and haltere from stage 12 onwards (Figure 7A) (Requena et al., 2017). Control experiments showed robust Antp immunoreactivity in the wing disc, with its highest levels in the hinge and A compartment (Figure 7B), in agreement with previous reports (Levine et al., 1983; Paul et al., 2021). In contrast, when Cas9 was expressed via *sna*1.7-Gal4 in the presence of *Antp* gRNAs, Antp immunoreactivity was severely affected, yet, only totally depleted in some of the discs (Figure 7C). Interestingly, some of these discs presented dramatic changes in the Ap pattern, presenting only isolated Ap-expressing clones (Figure 7C'). anti-Ap intensity in these clones was comparable to controls, suggesting problems in *ap* early pattern establishment rather than later maintenance of *ap* expression. Finally, in those discs without Antp immunoreactivity, no Ap was detected (Figure 7C''). These discs presented severe malformations and did not exhibit the normal notum-hinge-pouch structure of wild type wing discs. Many of these individuals died during development, with survivors presenting problems in notum closure (data not shown). Among those flies that hatched, most flies presented correctly patterned wings, while they remained inflated in many cases. Some of the most severely affected flies lacked most wing disc derivatives, including the wings and parts of the notum (Figure 7D). Halteres were always normal (Figure 7D), suggesting that the malformations arise due to the specific loss of *Antp* and not due Cas9 expression. The poor viability of the *sna*1.7-Gal4, *U6-Antp*.gRNAs flies suggest that the individuals that hatched correspond to those wing disc that were least affected by gRNA expression (Figure 7C).

These results reveal a fundamental role for Antp during early wing disc development, acting, at least in part, through the early activation of *ap.*

## Discussion

*Boundary position in the wing imaginal disc*

Boundary positioning is fundamental for proper development (Dahmann et al., 2011; Irvine & Rauskolb, 2001). Mispositioning of developmental boundaries leads to severe developmental defects. In the wing imaginal disc, the intersection between two developmental boundaries is responsible for the specification of the wing pouch and the establishment of the coordinates which regulate tissue patterning. In this study, we have analyzed the role of the apE enhancer in the correct establishment of the DV boundary. In previous studies, it had been shown that the EGFR pathway is a key input required for early *ap* transcription (Bieli, Kanca, Requena, et al., 2015; Wang et al., 2000; Zecca & Struhl, 2002). However, the expression pattern of the EGFR ligand *vn* is highly dynamic during the onset of *ap* expression: in L1 and L2 larvae, *vn* is expressed in a proximodistal stripe, both in future ventral and dorsal cells, which only later is confined to the proximal end of the wing disc (Paul et al., 2013). In contrast, *ap* is first expressed in the center of the wing disc, acquiring its characteristic pattern during the second instar (Nienhaus et al., 2012; Paul et al., 2013). Together, these patterns suggest a more complex regulatory scenario. In this study, we provide evidence that both Hth and Grn are required for apE activity (Figures 4D, 7). Interestingly, these two factors are expressed early in the presumptive hinge region (Brown & Castelli-Gair Hombria, 2000; Wu & Cohen, 2002) (See Figure 8 for a working model on *ap* regulatory inputs). In particular, Grn is enriched in the areas in which the transverse connective trachea is in contact with the wing (Guha et al., 2009). This extra layer of apE regulation might explain why the early expression of *ap* is initially confined to the central part of the wing, and why the first cells expressing *ap* are often located close to the trachea (Nienhaus et al., 2012). Remarkably, both Hth and Grn are also expressed in the ventral hinge, which implies that either these factors are not sufficient to activate *ap* expression or that their activity is actively repressed in this territory. Along these lines, the TF Optomotor-blind (Omb) has recently been proposed to repress *ap* expression in the distal wing (Chen et al., 2023).

Loss of EGFR signaling has also been associated with mirror image duplications (Baonza et al., 2000). However, the mechanism proposed was that EGFR maintains *en* expression in P cells. Interestingly, many of the duplications reported in this study mimicked those presented here (Figure 1). Given the fact that EGFR pathway activates apE (Bieli, Kanca, Requena, et al., 2015) and that the deletion of Pnt binding sites within apE also result in mirror image duplications (Figure 4B), we propose that the previously identified phenotypes arise due to apE miss regulation and not due to loss of *en* maintenance. To confirm whether this is the case, the lineage of *en*-expressing cells should be analyzed upon EGFR loss.

Furthermore, downregulation of JAK-STAT signaling has been shown to produce mirror image duplications (Recasens-Alvarez et al., 2017). The OR463 phenotypes described in Figure 1 also mimic those of JAK-STAT defects. *ap* is fundamental for the development of the hinge, where Upd-1, the ligand of the JAK-STAT pathway, is expressed (Johnstone et al., 2013). Hence, it is possible that *ap* expression indirectly disrupts JAK-STAT signaling by interrupting the production of its ligand. Alternatively, JAK-STAT mirror image duplications could arise from the direct regulation of apE. Interestingly, some STAT92E binding sites are predicted in N1 and N2 (data not shown). It is also possible that direct apE regulation via JAK_STAT signaling could result in duplications.

Although apE is active throughout the dorsal compartment, its disruption leads to a preferential loss of ap expression in posterior cells. The asymmetric effect of apE perturbation on the anterior and posterior compartments suggests that apE transcriptional control is not equivalent across the A/P axis. Compartment-dependent differences in enhancer regulation have also been documented in other developmental contexts; for example, the Distal-less DMX-R element is interpreted through distinct cofactor combinations (Sloppy paired anteriorly and Engrailed posteriorly) (Gebelein et al., 2004), and specific

mutations within DMX-R preferentially disrupt enhancer function in anterior versus posterior cells. It is possible that apE is more sensitive to misregulation due to differential transcriptional regulation across compartments. Nevertheless, we cannot exclude the possibility that the posterior bias we observe arises not from enhancer logic per se, but from intrinsic differences in tissue architecture or the dynamics of boundary positioning during wing disc development.

*A HOX-GATA complex involved in wing development*

The genetic control of wing specification is well studied and many of the factors involved have been characterized. With the exception of the JAK-STAT pathway (Recasens-Alvarez et al., 2017), most of the factors required for wing specification were identified more than two decades ago. Here, our bottom-up approach permitted us to describe the requirement of two additional factors for the development of the wing imaginal disc. Our data suggests that the GATA TF Grn is fundamental for wing development. *grn* was originally described as a gene involved in epithelial morphogenesis in the embryo and the legs. Here, we report that loss of *grn* also causes extreme phenotypes in the wing disc (Figure 6). Interestingly, we found that *grn* is not only important for activation of *ap*, but also for the growth and survival of the whole tissue. P compartments lacking *grn* were of very small size or totally lacking (Figure 6). However, their elimination occurred over a long period, during which the mutant cells were still able to instruct patterning and growth to their surroundings. Previously, mutant clones of *grn* covering the wing blade were reported not to produce any developmental defects (Brown & Castelli-Gair Hombria, 2000). The apparent difference between these results is likely to emerge from the different approaches used to eliminate *grn* function. While the previous study performed a clonal analysis using the the minute technique, here we knocked down *grn* using RNAi or knocked it out using a tissue-specific CRISPR. These two approaches resulted in a homogeneous loss of *grn* function in all posterior cells already in early embryonic stages, which is not the case for Minute clones. It is likely that this temporal difference is the main reason for these discrepancies, as we have also observed that *grn* clones generated late in development do not affect *ap* expression (data not shown), suggesting that Grn is only required during very early stages of wing development.

Most point mutations or short deletions in enhancer regions have little effect on gene expression. This robustness emerges, in part, from the collective action of TFs, whose binding sites are often clustered in groups. In addition, the deletion of enhancers which were thought to have central roles in development has often been found to have minor phenotypes due to existence of redundant sequences located in the vicinity (Lopez-Rivera et al., 2020). Even in *Drosophila*, examples of mutant phenotypes derived from point mutations in enhancers are rare (Shimell et al., 1994). Recent large-scale enhancer mutagenesis studies have shown that the mutational consequences within enhancers can vary widely. In some cases, many nucleotide positions appear tolerant to single-base changes and only a small subset of mutations produce clear functional effects (Kvon et al., 2020). In other enhancers, regulatory information is distributed more densely, and mutations at multiple positions can alter output (Fuqua et al., 2020). Together, these studies illustrate that enhancer sensitivity is not uniform but depends on enhancer-specific features such as motif organization, cooperativity, and redundancy. Within this broader landscape, the apE enhancer appears to represent a particularly sensitive case.

In this study, we have identified an area of the *Drosophila* genome with exceptional sensitivity to mutation. Four of our two-base-pair substitutions within the HOX binding site of m3 resulted in total loss of wings. In this study we propose that Antp is the HOX TF that binds m3. In support of this hypothesis, we demonstrated that early loss of *Antp* in the embryonic wing primordium results in defects in *ap* expression (Figure 7C'), in

severe cases leading to a total loss of Ap (Figure 7C''). Until recently, the second thoracic segment was assumed to develop independently from any HOX input. However, several groups have now reported that this segment, from which the wing is derived, requires the input of the HOX gene *Antennapedia* (*Antp*) for its development (Fang et al., 2021; Paul et al., 2021). These studies uncover a role of Antp during larval wing morphogenesis and wing margin formation. Given the severity of the phenotypes we observed (Figure 7C'', E), our experiments describe a much earlier role of this gene, most likely during wing disc specification. While we demonstrate the requirement of Antp for *ap* expression, whether this effect is direct and occurs through m3 binding site still needs to be confirmed with biochemical evidence. Hox TFs have been proposed to function as pioneer TF in some contexts, changing the enhancer's chromatin accessibility and enabling the binding of other TFs to the enhancer (Bulajić et al., 2020; Loker et al., 2021). Such pioneer Antp activity could explain the severity of the mutations in apE. However, biochemical characterization of the locus in early wing imaginal discs precursor cells is required to test this hypothesis.

The current working model for the functioning of OR463 includes two steps. First, Grn and a HOX TF, possibly Antp, would act on the enhancer, permitting its later activity. Then, during L1 and L2 stages, Pnt and Hth, probably together with other TFs, would confer the spatial clues that result in the early Ap activity. The mechanism of action of each factor in the enhancer remain to be investigated.

It is important to acknowledge that all expression analyses were conducted in third-instar discs, a stage that follows the initial establishment of *ap* expression. Earlier effects are therefore inferred rather than directly observed, as imaging and staging of early discs present significant technical challenges due to their small size and fragility. A direct observation of the early wing disc across mutant conditions would likely help to clarify the role of the discovered factors during early ap expression.

*New method to manipulate enhancers*

In the past decades, the functional analysis of enhancers depended on the generation and analysis of lesions in the respective DNA fragment, often studied with reporter transgenes, in which the mutated enhancer was fused to a minimal promoter driving the expression of a reporter gene (LacZ, GFP, etc.). Such analyses provide an idea of the spatio-temporal changes in enhancer function when the enhancer is mutated. Minimal reporter fusions have been fundamental to characterize enhancers; however, follow up studies of such mutation analyses using endogenous gene editing often demonstrates minor effect for many mutations when analyzed in their endogenous genetic environment. Moreover, this approach does not permit to manipulate and characterize the requirement of a particular binding site in time and space. In recent years, the advance of techniques based on catalytically dead Cas9 (dCas9) has opened the door for the precise somatic disruption of enhancers. Enhancer repression has been mainly accomplished by dCas9-mediated recruitment of epigenetic repressors (Wang et al., 2016). However, the precision of this approach is hard to measure and depends on the repressive element to which dCas9 is fused. dCas9 binding to specific sites has also been shown to be sufficient to disrupt TF-DNA binding in prokaryotes (Qi et al., 2013) and in cell culture (Shariati et al., 2019), opening the door to a more precise manipulation of selected DNA regions or sites. Here, we adapted the latter approach for its use *in vivo* in *Drosophila*. We demonstrate that the sole expression of dCas9 together with gRNAs binding OR463 is sufficient to mimic the phenotypes caused by endogenous enhancer mutants. Moreover, the localized expression of dCas9 permitted us to show that the mirror image duplications arise due to the early defects in the activity of the enhancer in the P compartment and that to delimit the temporal window of enhancer function.

This approach has broad applicability and might be useful to investigate the importance of regulatory sequences across the *Drosophila* genome. The ease by which gRNA expressing stocks are generated (Port & Bullock, 2016) and the possibility to encode many gRNAs in a single transcript will further simplifies the functional characterization of enhancer regions.

## Materials and methods

*Fly strains and husbandry*

The following fly strains were used in this study: *vasa*-Cas9 (Bloomington number: BL51323), $ap^{DG3}$ (Bieli, Kanca, Gohl, et al., 2015), $ap^{DG12}$ (Bieli, Kanca, Requena, et al., 2015), *en*-Gal4 (gift from Manuel Calleja), *ptc*-Gal4 (BL2017), *sna*1.7-Gal4 (Requena et al., 2017), G-TRACE (BL28281), *UAS*-CD8:GFP (BL32186), *upd1*-Gal4 (gift from Prof. Denise Montell), *UAS*-EGFP (BL6874), UAS-*pnt*RNAi (BL35038), UAS-*hth*RNAi (BL34637), UAS-*grn*RNAi (BL27658 and BL34014), *UAS-dicer*; *en*-Gal4, UAS-2xEGFP (BL25752), apE-LacZ (Bieli, Kanca, Requena, et al., 2015), U6-*grn.*gRNA (BL85866), *UAS*-Cas9 (BL58986), *grn*:GFP (BL585483), *tub*-$Gal80^{ts}$ (BL7016). The stocks generated in this study are listed in Supplementary Table 1. Flies were kept at 25C° unless specified and were fed using home-made polenta supplemented with yeast.

*Immunostainings and image acquisition*

For immunostaining, larvae of the desired stage were dissected in ice cold PBS (pH 7,2, GibcoTM) and immediately transferred into paraformaldehyde (PFA) solution (4% PFA in PBS) for 30 min at room temperature. The dissected tissues were washed 2x15min with PBST (0,3% Triton-X in PBS) to permeabilize the tissue, followed by a 1h incubation in blocking solution (5% Normal Goat Serum in PBST. Subsequently, samples were incubated in primary antibody diluted in blocking solution at 4C for 16h. The next day, the samples were washed 3x15 min with PBST and incubated for 2 hours in the secondary antibody diluted in blocking solution. Finally, samples were washed 3x15min with PBST, followed by 2x15min washes with PBS. All the steps were performed at room temperature using gentle rotation unless specified. Samples were mounted using Vectashield mounting medium (with or without DAPI) on a glass slide, covered with a cover-slide (n1.5) and sealed using nail polish. Images were then acquired using a Zeiss LSM880 point confocal microscope and analyzed using ImageJ.

*Antibodies*

The following primary antibodies were used in this study: Rabbit anti-Ap (1/750) (Bieli, Kanca, Requena, et al., 2015), mouse anti-En (1/30, clone 4D9 DSHB), anti-Ptc (1/150, Apa1.3 clone, gift from Prof. Isabel Guerrero), anti-Hth (1/500, gift from Natalia Azpiazu), anti-ß-Galactosidase (1/1000, Abcam AB9361), anti-Wg, 1/120) (Clone 4D4, DSHB), Anti-Antp (1/15, Clone 8c11, DSHB) Anti-Vg (1/100, gift from Prof. Kristen Guss) The secondary antibodies employed were: goat anti-rabbit IgG (H+L) Alexa Fluor 680 (A-21109; Thermo Fisher), F(ab`)2-goat anti-rabbit IgG (H+L) Alexa Fluor 568 (A-21069; Thermo Fisher), goat anti-mouse IgG (H+L) Alexa Fluor 568 (A-11004; Thermo Fisher), Alexa Fluor 680 AffiniPure goat anti-mouse IgG, Fcγ fragment specific (115-625-071; Jackson ImmunoResearch).

*Generation of OR463 landing site*

Easy genetic screening of successful CRISPR/Cas9-mediated HDR-genome editing events is possible if an appropriate dominant selectable marker is available. Towards that end, we have adapted a feature of the dominant *apterous* allele $ap^{Xasta}$ (D. Bieli et al., 2015a). This allele is caused by a reciprocal translocation

between the chromosome arms 2R and 3R that brings together the *ap* regulatory region and the *dad* (*daughters against dpp*) locus. *dad* is expressed in the wing disc in response to *dpp* signalling (Weiss et al., 2009). Due to the translocation, the wing-specific *dad* enhancers DadInt52 and Dad4 are located close to the *ap* promoter. This leads to ectopic *ap* expression in the ventral wing disc compartment that elicits the typical *Xasta* wing phenotype. Heterozygous flies show a dominant phenotype where the distal part of the wing is lost and a mitten shaped wing is formed. We have shown that when engineered into the *ap* locus, *dad* enhancers DadInt52 and Dad4 are sufficient to induce the dominant Xa-phenotype (Bieli et al., 2015a). Based on these observations, it was decided to clone a sub-fragment of Dad4, Dad13, into the donor plasmid used for CRISPR-mediated homologous recombination (HDR). Dad13 is only 517 bp long and has been shown to contain all necessary sequences for *dpp*-dependent activation (Weiss et al., 2009). Consequently, it was expected that introduction of the Dad13 fragment into the *apterous* locus would induce a dominant wing phenotype. Thus, flies displaying this phenotype could be expected to contain successful homologous recombination events.

To generate the donor plasmid used as a template for HDR repair, a fragment containing the homology arms (each 536 bp long), an attP site (55 bp), two FRTs (34 bp each) flanking restriction sites AvrII and EcoRI and gRNA targets for linearization, was synthesized by Genewiz and cloned into pUC57-Kan. This plasmid is named pDB350. Subsequently, the 517 bp Dad13 enhancer was amplified from plasmid pDB45 using the primers 5'-CCCCCCTAGGCCTCAACCTTAAATTGTTG-3' and 5'-CCCCGAATTCCGAACGGGAGAGCGCCGC-3' and cloned by restriction ligation into the aforementioned plasmid using the sites AvrII and EcoRI (underlined). The final donor plasmid is called pMS358. In addition, two plasmids encoding gRNAs targeting OR463 were generated (pA359 and pA360). The following primers were annealed and cloned into pU6-BbsI-chiRNA (Gratz et al., 2013) that was digested with BbsI: 5'-CTTCGCAGGCTCTGCCGAAGGTTCA-3' together with 5'-AAACTGAACCTTCGGCAGAGCCTGC-3' and 5'-CTTCGTCAGAACGGTCAGCTACCTG-3' together with 5'-AAACCAGGTAGCTGACCGTTCTGAC-3'. gRNA targets were identified using CHOPCHOP (Labun et al., 2019).

After injection of the three plasmids into *y w vas-Cas9;* + embryos, surviving adults were individually crossed with *y w* flies. From these, 67 fertile F1 crosses could be screened for flies with wing defects. Successful HDR events could be isolated from four of the 67 G0 crosses (6%): c25, c77, c94 and c102. Alignment of the sequencing data with the *in silico* designed genomic sequence showed that candidates from all four crosses contained the expected changes down to the last base pair: the attP-FRT-Dad13 enhancer-FRT fragment is inserted in place of the 463 bp OR463 enhancer fragment. The sequence immediately flanking the inserted cassette (indicated by -[]-) is: CCCCTCGAATCGATTCAAAT-[]-TATAATTTGACCGCAATTTT. On the distal side, the break coincides with the $ap^{Xa}$ break point.

As a result of the insertion of the Dad13 enhancer, it was expected that successful HDR-events would show an easy to spot phenotype similar to that in $ap^{Xasta}$/+ flies. This was the case for some candidates isolated from cross c94. Although the phenotype is somewhat less pronounced, the tip of all wings always shows an obvious indentation (Figure 1 – figure supplement 3A'). The dominant phenotype is much more subtle and less penetrant in other c94/+ candidate wings (Figure 1 – figure supplement 3A'). In these and in candidates from the other three crosses, only a tiny spike of wing tissue emerges near the tip from the ventral side of the wing. We have previously observed a very similar phenotype in dpp-Gal4>UAS-dad flies (Bieli, Kanca, Gohl, et al., 2015). We have no explanation why insertion of the Dad13 enhancer gives rise to these different wing phenotypes.

From several of the candidates, the Dad13 enhancer was removed by Flp treatment. In all cases, homozygous *ΔDad13* derivatives were viable and fertile. Importantly, they also had no wings and halters,

indicating that the designed deletion is a perfect starting point for our *in-situ* analysis of the apE wing enhancer. HDR-event c94.19 was chosen as landing site for mutated OR463 fragments and a *y w vas-integrase; c94.19$^{\Delta Dad13}$/CyO* stock was established. In this study, this landing site is referred to as *ap$^{R2}$*.

*Generation of OR463 rescue fragments*

Most of the small deletions were engineered according to the method described by(Pérez-Pinera et al., 2006). A pBlueScript plasmid containing OR463 (pDB51) served as a template for the creation of these deletions. All primers used for this purpose are listed in Supplementary Table 2. OR463 fragments containing more than one deletion (*Δm1m4* and *Δm1m2m4*) were generated step by step. At the end, all mutated OR463 fragments were amplified using the primers: 5'-TCAAGCTTTCCAGCTCTGAATCTCACTCCC-3' and 5'-GTACTAGTGGAGGCCAGCTCTAAAATCG-3'. Subsequently, amplified fragments were cloned into the re-entry plasmid pDB345 using the restriction sites HindIII and SpeI (underlined). All plasmids destined for transgenesis were verified by Sanger sequencing.

Several OR463 derivatives including the m3.1 substitution library were synthesized and cloned by Genewiz (see Supplementary Table 1).

One of the deletions was obtained as a NHEJ-byproduct when generating the *ap$^{R2}$* landing site. It is *ap$^{N5}$* (isolation number c102.1). It contains a 19 bp deletion created at the site of the distal gRNA cutting site. The sequence flanking the deletion (indicated by -[]-) is as follows: TTTCGTGTGATTTCGGGACC-[]-GTTCTGATCTCGGCTACAAA. Note that this allele is not associated with flanking attL and FRT sites.

Re-entry plasmid pDB345 consists of the following parts. The backbone is pUC57-KanR. In contains an attB site (54 bp) and a 35 bp polylinker consisting of the following unique restriction sites: HindIII_PacI_NheI_XhoI_MluI_SpeI. A 48 bp extended FRT site precedes *mini-yellow*, which serves as selectable marker. It is a 2650 bp KpnI/ClaI fragment mainly consisting of a yellow cDNA devoid of all known *yellow* enhancers. When inserted in the *apterous* locus, *mini-yellow* is expressed mainly in the wings of transgenic flies. However, its presence interferes with apterous function. In hemizygous *ap$^{R2\text{-}WT[y+]}$/ap$^{DG3}$* flies, 94% of the wings showed a phenotype, which was usually restricted to the posterior wing compartment. Frequently, an enlargement of the posterior compartment could be observed (see Figure 1 – figure supplement 3C'). This phenotype is reminiscent of *ap$^{blot}$* (Whittle, 1979)This allele carries a *blood* retrotransposon 140 bp proximal to the distal end of OR463 (Bieli, Kanca, Gohl, et al., 2015). It is conceivable that the presence of *blood* or the *mini-yellow* marker (including the pDB345 backbone) within 55 bp or 195 bp, respectively, of the crucial m3 region is responsible for the phenotypic effect. Thus, the *mini-yellow* marker was removed by Flp-treatment from all *ap$^{R2}$* transgenic inserts presented in this study. At the end of this procedure, the foreign DNA flanking OR463 fragments are the 56 bp attL on the proximal and the 34 bp FRT on the distal side. Importantly, removal of the foreign DNA led to a dramatic increase in hemizygous *ap$^{R2\text{-}WT}$/ap$^{DG3}$* flies with normal wings. Most homozygous *ap$^{R2\text{-}WT}$* flies developed normal wings. Few of them can have weak phenotypes like small notches and other weak margin defects or blisters (see arrow in Figure 1 – figure supplement 3D'). In hemizygous *ap$^{R2\text{-}WT}$/ap$^{DG3}$* flies, 95% wings are normal. The remaining wings can also show the enlarged posterior compartment phenotype seen in hemizygous *ap$^{R2\text{-}WT(y+)}$* flies. It is possible that the remaining attL and FRT sites impede with complete rescue of the wing phenotype. Nevertheless, wing phenotypes of *ap$^{R2}$* and *ap$^{R2\text{-}WT}$* warrant a faithful dissection of the OR463 enhancer.

From a practical point of few, it might be of interest with what efficiency all the m3.1 substitution library transgenes were obtained. The library contains 22 different plasmids (1 wild-type and 21 mutants; synthesis

and cloning by Genewiz)). After injection of the plasmid mix into *y w vas-integrase; ap$^{R2}$/CyO* embryos, survivors were reared to adulthood and individually crossed with y w partners. From 34/141 fertile G0 crosses, 248 y$^{+}$ transformants were selected. These were individually crossed with *y w ; ap$^{DG3}$/CyO, Dfd-YFP* partners. After a few days, the y$^{+}$ candidates were sacrificed and screened by PCR and sequencing. PCR primers were A185 (5'-CACCTGACTCAATAGCAAGACT-3') and m2 (5'-CAGTGTTCGGGTAATCAGGTG-3'). The resulting 1227 bp product was sequenced with primer P41 (5'-CTAATGCAATCGACAAACCCC-3'). After screening 104 randomly chosen candidates, all 22 possible alleles were represented by at least one candidate.

*Generation of the UAS-dCas plasmid, OR463 gRNAs and control gRNA*

The ORF of FLAG-NLS-dCas9-NLS was amplified from the plasmid pWalium20-10X*UAS*-3XFLAG-dCas9-VPR (Addgene: #78897) (Lin et al., 2015) using the primers: 5'-*ATCGCGGCCGCCGCCACCATGGATTACAAG*-3' and 5'-*GTGGTACCTCACACCTTCCTCTTCTTCTTGG*-3'. The fragment was subsequently cloned into the pUAStattB plasmid using the restriction sites NotI and KpnI.

U6-OR463x4 was generated using stablished protocols using the pCFD5 vector (Port & Bullock, 2016). sgRNA spacer sequences were (in 5' to 3' order within the array): 1) 5'-*TCACTCCCAGGCTCTGCCGA*-3', 2) 5'-*TCCAGAGATCGAGCGTCAGT*-3', 3) 5'-*ATTTGTAGCCGAGATCAGAA*-3' and 4) 5'-*AAAATATATGAATCCATTGC*-3'. As control gRNA, we used a gRNA binding an unrelated sequence in the iab5 regulatory region of *AbdB*. The gRNA was cloned following published protocols (Port & Bullock, 2016). The spacer sequence was: 5'-*GTTGAGTTAGAGATCCCAGCAGG*-3'.

The pCFD5-OR463.gRNAx4 plasmid was injected in the BL25709 to generate flies used in this study.

*Generation of gRNAs targeting the Antp locus*

U6-OR463x4 was generated using stablished protocols using the pCFD5 vector (Port & Bullock, 2016). sgRNA spacer sequences were (in 5' to 3' order within the array): 1) 5'- *CTAGCTCTAGAGTCTGGTAC*-3', 2) 5'- *ATGACGCTGCCCCATCACAT*-3' and 3) 5'- *GTACGAGTTGGTGAAGTACG*-3'. The pCFD5-*Antp*.gRNAx3 plasmid was injected in the BL25709 to generate flies used in this study.

*Generation of CON2 and CON5 fluorescent reporters.*

mKate:NLS and eGFP:NLS fragments were synthesized by Genewiz and cloned via AgeI/SacII into pAttB-C2-LacZ and pAttB -C5-LacZ (Bieli, Kanca, Requena, et al., 2015), respectively. Such as the LacZ ORF was substituted by that of the fluorescent proteins.

*Generation of Antp MARCM clones*

Eggs of the indicated age were given a heat-shock at 37º degrees for one hour in a water bath. After incubation, tubes were transferred to 25 degrees until dissection. The genotyped of the flies was:

*y, w, hs-FLP, tubGal4, UAS-GFP /+ ; ; Antp$^{NS+RC3}$, FRT82B/ ubi-GFP, FRT82B*

*Statistical analysis*

The statistical analyses performed in Figure 2 were t-test. Prism software was employed to analyze the data and generate the graphs. P-values are indicated the figure legend.

*X-Gal staining*

Third instar larvae were dissected in cold PBS by ripping the most anterior third of their cuticule and removing the internal organs. The cuticle was then reverted to expose the wing discs to the exterior. The tissues were fixed by incubation at RT for 15 min in 1% glutaraldehyde (Fluka) (in PBS) and subsequently wash them with 0.1% Tween 20 (Fluka) in PBS under roation at RT. Samples were then incubated using staining solution (440µ $H_2O$, 25µ 200mM $NaP_i$ (pH 7.2), 15µL 5M NaCl (in $H_2O$), 0.5µL 1M $MgCl_2$, 5µL 333mM $K_4[Fe^{II}(CN)_6]H_20$, 5µL 333mM $K_3[Fe^{III}(CN)_6]H_20$, 2.5µL 10% Tween-20, 8µL 5%X-Gal (appliChem) in dimethylformamide) at 37degree in the dark for 90min. Finally, samples were washed with 0.1% Tween 20 and with PBS before mounting in 80% glycerol on a microscope slide.

*Bioinformatical analysis of apE*

Sequence conservation of the OR463 fragment within the *ap* upstream intergenic region was analysed across different dipteran species using the "Cons 124 Insects" multiple-alignment track of the *D. melanogaster* dm6 genome on the UCSC Genome Browser (Kent et al., 2002, https://genome.ucsc.edu). Conservation scores were obtained from the phastCons (Siepel et al., 2005) and used to delineate conserved and less conserved blocks within OR463. Conserved transcription-factor binding sites were predicted with MotEvo (Arnold et al., 2011), which defined four conserved modules (m1–m4) and six inter-modules (N1–N6). Additional motif analysis was performed using the JASPAR CORE Insecta database and the Target Explorer tool to cross-validate conserved binding-site predictions and refine motif assignments within the enhancer.

## Figure legends

**Figure 1. Two conserved regions within OR463 are fundamental for wing development. A.** Illustration of *ap* upstream intergenic region. In blue: enhancer sequences relevant during wing development (Bieli, Kanca, Requena, et al., 2015). In black: OR463 sequence conservation among related insects. **B.** Different regions in which OR463 was divided for mutation analysis. In dark grey, sequences with highly conserved TF binding sites. **C.** Percentage of wild-type wings when each of the fragments was deleted in homozygosis and (**D**) hemizygosis (over the $ap^{DG3}$ allele). **E.** Control wing (Re-integrated WT OR463 in $ap^{R2}$ landing site). **F.** Loss of wing displayed by *ΔOR463* mutants. **G.** Loss of wing displayed by *Δm3* mutants. **H.** Representative wing phenotype derived from *Δm1* deletion in homozygosis. Anterior compartment presents correct venation, while P compartment presents an outgrowth. Venation pattern in this outgrowth is disturbed. Inset 1: Detail of the A compartment bristles. Inset 2: bristles of A identity in the P compartment. **I.** Representative wing phenotypes derived from *Δm1* deletion in hemizygosis. P compartment venation pattern is disturbed. No outgrowth is formed but the P compartment present severe venation problems, with some veins position perpendicularly to its normal direction. Inset 1: Detail of A bristles. Inset 2: Detail of A bristles in the P compartment. Note that transformation of the P margin into A is not complete. **I'.** Wing phenotype also present in *Δm1* hemizygous flies. In these, the P compartment is severely reduced and mostly A bristles are present in the margin.

**Figure 2. Mirror image duplications arise due to changes in DV and AP boundary position. A.** Anti-Ap and anti-Wg immunostaining of control wing discs (Re-integrated WT OR463). **A'.** Anti-Ap and anti-Wg staining of wing discs in homozygous *Δm1* mutants. The DV boundary is distorted in the P compartment, where it is extended into the presumptive wing hinge (arrowheads). **A''.** Anti-Ap staining of *Δm1* hemizygous wing discs. The DV boundary is further deformed in the P compartment (arrowhead). **B.** Quantification of the relative P size (P Area/Total Area) and relative PD size (PD Area/Total Area) in different mutants (p value<0.0005, control: n=13, N1/DG3: n=16, *Δm1*/DG3: n=10, *Δm1m2m4*/DG3: n=9). **C, C' and C''.** Relative position of AP and DV boundaries as revealed by immunostaining with

anti-Ap and anti-Ptc in wing discs of control, *Δm1*/DG3 and ΔN1/DG3. Different quadrant maps are then subtracted and the AP and DV boundaries represented with dashed lines (red and blue, respectively). Asterisk depict the intersections of AP and DV boundaries. Scale bars: 100μm. **D.** Schematic of wild-type wing development from larval to pupal stages. In the larval disc, the AP boundary (green) intersects the DV boundary (purple) at a single point (asterisk). During pupal eversion, the wing pouch unfolds along the DV boundary, which becomes the future wing margin, and veins are patterned in parallel to the AP boundary. The arrow marks the region where AP and DV boundaries overlap within the posterior compartment. **D'.** Model in which PD growth is strongly reduced or nearly absent. After eversion, the anterior compartment will present anterior identity on its dorsal side and posterior identity on its ventral side. This mixed orientation accounts for the partial A identity observed at the posterior border. **D''.** Model in which PD size is reduced but still occupies a considerable pouch area. Here, the AP and DV boundaries meet at two distinct positions within the pouch, spaced far enough apart to support the specification of two wing organizing centers. After eversion, the secondary center generates a wing structure with dorsal A identity and ventral P identity, producing characteristic venation defects patterned along the ectopic DV boundary.

**Figure 3. Spatiotemporal characterization of OR463 via localized dCas9 expression. A.** Schematic representation of the method. Upon localized expression, dCas9 would bind to DNA displacing or interfering with the binding of TF. **B.** Target sites of the gRNAs present in the *U6*-OR463.gRNAx4 transgene. **C.** Wings of animals expressing dCas9 under the *en*-Gal4 driver in the presence of the control gRNA at 23º and 25º degree. **D.** Wings of animals expressing dCas9 under the *en*-Gal4 driver in the presence of *U6*-OR463.gRNAx4 at 23º and 25º degree. Arrowhead indicates the P outgrowth. Notice the presence of A bristles in the P edge (dashed box). **E.** Control wing discs, expressing dCas9 under the *en*-Gal4 driver in the presence of control gRNAs at 23º. **E'.** Anti-Ap immunostaining showing the normal Ap expression pattern in late wing discs. **E''.** Quadrant map subtracted from panel E. Notice the single perpendicular intersection between AP and DV boundaries. **F**. Anti-Ptc and Anti-Ap immunostaining of wing discs expressing dCas9 under the *en*-Gal4 driver in the presence of *U6*-OR463.gRNAx4 at 23º. Notice the P outgrowth (arrowhead). **F'.** Anti-Ap immunostaining exhibiting the extended posterior pattern in the posterior compartment. **F''.** Quadrant map subtracted from panel F. Notice reduce size of PD quadrant. AP and DV contact twice, once perpendicularly as in control discs and once tangentially in the P outgrowth. **G.** Anti-Ptc and Anti-Ap immunostaining of wing discs expressing dCas9 under the *ptc*-Gal4 driver in the presence of *U6*-OR463.gRNAx4 at 23º. Notice lack of Ap signal along the central wing disc (asterisk). **G'.** Anti-Ap immunostaining of the disc in G. **G''.** Quadrant map subtracted from panel F. Notice the lack of contact between AD and PD quadrants. Scale bars: 100μm. **H.** Schematic of the temperature-shift experiment used to define the developmental window during which the apE enhancer is sensitive to repression. *en*-Gal4, *tub*-Gal80$^{ts}$, UAS-dCas9; *U6*-OR463.gRNA(4×) animals were kept at 18 °C to suppress dCas9 and shifted to 29 °C at successive developmental intervals (0–168 h AEL) to induce dCas9 expression at distinct stages. **H′ .** Timeline summarizing the temperature regime and the percentage of adult wings showing strong apterous-like phenotypes following induction at each time point. Early induction (0–48 h AEL) produced the highest penetrance, with progressively weaker effects after 72 h AEL.

**Figure 4. Pnt and Hth are required for apE activity via m1. A.** Schematic representation of m1 and m4 predicted binding sites and the generated deletions within m1. **B.** Phenotypic penetrance of the different deletions within m1 in homozygosis, and hemizygosis (**B'**). **C.** Projected area of the different quadrants of control (WT/*ap$^{DG3}$*, *Δm1*/ *ap$^{DG3}$*, *Δm1.2*/ *ap$^{DG3}$* and *Δm1.3*/ *ap$^{DG3}$* wing discs, based on the immunostaining against Ap and Ptc in real wing discs. **D.** Effect on the Ap expression domain by the expression of *hthRNAi* and *pntRNAi* in the P domain using *en*-Gal. In both cases the PD domain is reduced. In green, the *UAS*-CD8:GFP reporter marks the P compartment. **E.** Adult wing phenotypes upon *pntRNAi* expression via *en*-Gal4. Left wing: Example of a wing outgrowth resembling *Δm1* phenotype. Middle wing: Example of a partial A mirror-image transformation. Inset 1: campaniform sensillae of the A compartment. Inset 2: ectopic campaniform sensillae formed in the P compartment upon *pnt*RNAi expression. Notice the presence of A bristles within the P compartment. Right wing: Example in which P compartment is reduced. **F.** Effect of the expression of *hthRNAi* and *pntRNAi* in the P domain on anti-Ap localization and apE-LacZ reporter (visualized with anti-ßGal) during L2 stage. In control discs, anti-Ap can be detected in the nucleus of P cells (marked with *UAS*-CD8:GFP) (arrowheads). anti-ßGal (in white) is detected in the dorsal compartment in both A and P compartments.

Upon *pntRNAi* or *hthRNAi*, no anti-Ap nor anti-ßGal signal was detected in P cells (arrowheads). Scale bars: panels C and D, 100μm; panel E, 25μm

**Figure 5. High resolution genetic analysis suggests a HOX-GATA complex important for m3 activity. A.** anti-Ap and anti-Wg immunostaing in control and *Δm3* third instar wing discs. In contrast to control wing discs, Ap can only be detected in a small group of cells in the anterior hinge in *Δm3* mutants (arrowhead). The territory within Wg inner ring is totally missing (asterisk). No Wg stripe is detected in the pouch. **B.** X-Gal staining of control apE-LacZ and apEΔm3-LacZ in third instar wing disc. apEΔm3-LacZ only showing minimal X-Gal staining in the P hinge. **C.** Summary of the base pair substitutions generated within m3.1. Each row corresponds to a different allele containing the changes labelled in red. **D.** Scoring of wild-type wings across the library of *Δm3* mutants. In black, the percentage of WT wings. Between 80 and 250 wings were scored in each case. Asterisks denote mutants that gave rise to no wings with different penetrance. **E-E'''.** Wing phenotypes of the control, and three of the mutants of the library. **F.** Phenotypic penetrance scoring of control animals and individuals in which the linker between GATA and HOX binding sites was extended or contracted. **G**. Percentage of flies with wings upon deletion of m3, or deletion of m3 and simultaneous contraction of m2 linker. Scale bars: 100μm

**Figure 6. the GATA TF Grain is fundamental for wing development. A.** Phenotypes produced upon *UAS-grnRNAi* expression driven by en-Gal4 in the presence of *UAS*-dicer. Reduction of the P size and partial P to A transformation (evidenced by the campaniform sensilla in the P territory (arrowhead)). **A'.** Mirror image duplication of an anterior proximal rudimentary wing structure. **A''.** Thorax defects observed in some of the adults. **B.** Anti-Ap and anti-Wg immunostaining of control wing discs and P knockdown of *grn* (*grn*RNAi driven by en-Gal4). In both cases, *UAS*-GFP was used to mark P cells and *UAS*-dicer was included to increase knockdown efficiency. **B'.** Example of wing disc in which the P compartment (arrowhead) was located close to the DV boundary. In these cases, the pouch was specified and grew to some extent, as revealed by the space within the inner ring of Wg (asterisk). **B''.** Example of wing disc in which the remanent of the P compartment (arrowhead) is located close to the notum. Here, the notum primordium grew until a considerable size and presented the characteristic Wg band, indicating, to some extent, correct patterning. The pouch (asterisk) is completely absent. **C.** anti-Ap immunostaining upon tissue-specific knock-out of *grn* in the P cells using *en*-Gal4, UAS-Cas9 in the presence of *U6-grn*.gRNAs. *UAS*-CD8:GFP labelled posterior cells. Notice the total loss of P compartment in mid L3 wing discs (illustrated by the complete absence of GFP signal). **D.** L2 wing disc of the same genotype as in C. Immunostaining of apE-LacZ using anti-ßGal4, as well as anti-Ap reveals total lack of signal in the P cells. Scale bars: panels B and C, 100μm; panel D, 25μm

**Figure 7. The Hox gene *Antp* is fundamental for early wing development and *ap* expression. A.** Scheme of the experimental setup to delete *Antp* during early stages of wing development. *sna*1.7-Gal4 driver is used to express Cas9 in the embryonic precursors of wing and haltere. Cas9 is targeted to the *Antp* locus by three gRNAs (labelled with an arrow). Position of the homeodomain within *Antp* sequence is also indicated. **B.** Anti-Antp and anti-Ap immunostaining in control third instar wing discs. Notice the distribution of Antp throughout the disc, with its highest levels in the A compartment and hinge, and the faint band along the DV boundary. **C.** Example of wing disc derived from *sna*1.7-Gal4 driven Cas9 in the presence of *U6-grn*.gRNA. In this case Ap presented a rather normal distribution in the tissue. Antp could be still detected in the wing discs, amid a reduction of its levels. **C'.** Wing disc of the same genotype as C presenting severe problems in the Ap expression pattern. Ap was detected in the pouch only in two groups of cells (marked with an arrowhead). **C''.** Example of a wing disc of the same genotype as C and C'' in which no immunoreactivity against Antp is detected. Note the complete lack of the anti-Ap signal. In grey, DAPI. These discs lack all recognizable structures (no notum, and no pouch). **D.** Adult phenotype arising from the same genotype as B (control). The haltere is marked by an asterisk. **E.** Example of a severe case in which *Antp* was knocked out from the wing primordia (same genotype as in C, C' and C''). In this case, only a small portion of the right notum in still present, with the total loss of the right wing (arrowhead). Left wing presents severe morphological defects and forms a balloon-like structure. Further analysis of this wing revealed the presence of campaniform sensillae and A bristles in the P compartment (data not shown). Notice that the halteres were unaffected (asterisk). Scale bars: 100μm

**Figure 8. Working model for OR463 regulatory inputs.** During late embryonic or early larval stages, the HOX input in m3, possibly Antp, would be responsible of OR463 activation. During this early phase the enhancer is not yet

functional and the HOX could be priming the enhancer, permitting the later action of the other factors. Grain would participate in this process but its requirement is less critical than that of the HOX. Pnt and Hth would then, during L2 larval stage, activate apE first in the proximal area of the wing disc. Grn could also play a role in this early activity, confining the activity of *ap* to the dorsal hinge.

## Figure supplement legends

**Figure 1 – figure supplement 1. C2 and C5 activity throughout larval development. A.** illustration of *ap* locus. *ap* coding region is highlighted in dark grey, C2 in red and C5 in green. Within them, apE, OR463 and apDV are labelled in black. **B-H.** Wing discs of C2-mKate2 (red) and C5-eGFP (green) animals dissected at the indicated stages and immunostained for anti-Wg (blue). In early stages, only C2 is active in the central part of the tissue (B). C2 activity peaks in mid L2 (C) to later decrease and eventually disappear (G-H). C5 activity starts in few cells at the DV boundary (C) and later expands to all the dorsal pouch and part of the dorsal hinge (D-H). **B'-H'.** anti-Wg signal of the panels B-H. Scale bars: B-F: 20μm G-H: 50μm.

**Figure 1 – figure supplement 2. Identification of the minimal apE enhancer within apC2. A.** Eight DNA fragments from the apC2 region are shown. Their names are given on the left of the panel and their length in bp is indicated. These fragments were tested with two in vivo assays. (1) The fragments were introduced into reentry plasmid DB59 where they are combined with apC5 (contains apDV). These plasmids were brought back into landing site $ap^{attP\Delta Enh}$ (Bieli et al 2015). Stocks were established and their rescue potential was scored in hemizygous flies (over $ap^{DG3}$). (2) The fragments were cloned into a LacZ reporter plasmid and inserted into the zh-86Fb landing site. Their LacZ activity was assayed by standard procedures. **B.** The rescue activity of each allele is shown. +: normal wings are formed. nd = not done. **C.** The LacZ activity of each reporter construct is shown. +: normal apterous expression pattern in the wing imaginal disc. -: no LacZ activity. nd = not done. Based on these experiments, fragment OR463 was chosen as the minimal apE fragment.

**Figure 1 – figure supplement 3. Generation and validation of the OR463 landing site. A.** Schematic representation of CRISPR- mediated targeting of OR463. Embryos were injected with plasmids encoding for two gRNAs (red) laying within the OR463 fragment (blue box) to direct Cas9 to the locus. A donor plasmid was co-injected to serve as template during HDR. The donor plasmid contained: 1) the *attP* site (dark blue), 2) Dad13 minimal enhancer (517bp in green), flanked by FRT sites (red) in identical orientation, 3) homology arms (each 536bp long) to trigger integration via HDR, 4) flanking gRNA targets to linearize the donor plasmid inside the embryos. **A'.** Dominant wing phenotype of animals in which dad13 was integrated in *ap* locus. These animals presented variable phenotypes despite all having the same insertion. Phenotypes ranged from almost wild-type wings with small border defects in the distal tip (Lower wing, with detail of the tip) to a partial phenocopy of the classical Xasta indentations (upper wing). **B.** Dad13 was then excised by the action of Flp. **B'.** Homozygous wing phenotype of flies in which OR463 has been substituted by the landing site. **C.** Scheme of the re-integration of wild-type OR463 into the landing site. Re-integration constructs contained: 1) an *attB* site, 2) the OR463 sequence, 3) an FRT oriented as that in the landing site, 4) a mini-yellow marker. After insertion via φ C31 integrase, $y^+$ transformants were used to establish stocks. In a second step, the $y^+$ marker was deleted by Flp tratment. **C'.** Hemizygous wing phenotype of flies containing the reintegrated WT OR463 sequence before removal of the mini-yellow marker. These wings often presented aberrant phenotype, which included mirror-image A wing duplications. **D**. Final arrangement of the locus after Flp-mediated excision of mini-yellow. **D'.** Wing phenotype when wild-type OR463 sequence was re-inserted in the OR463 landing site after mini-yellow excision (in hemizygosis).

**Figure 2 – figure supplement 1. Ap localization in various genotypes.** Anti-Ap immunostaining in different OR463 mutants. Notice the deformation of the DV boundary in the P compartment in *ΔN1*/ $ap^{DG3}$, *Δm1* and *Δm1*/$ap^{DG3}$. In *Δm1m2m4* (note that m3 is still present in this genotype), the Ap expression pattern is severely reduced, apparently missing from the P compartment**.** Scalebars: 100μm

**Figure 2 – figure supplement 2. Loss of *en* expression cannot explain the mirror-image duplications of apE mutants. A.** Anti-En staining in wild-type and $\Delta ap^E$ mutants in hemizigosis ($\Delta ap^E$/ $ap^{DG3}$). While the wing disc size of

*Δap$^{E}$* mutants is affected, En localization is still constrained to the P side and there is not dramatic change in its pattern**. B.** Control and **C.** *Δm1* hemizygous wing discs in which the current expression of *en* (Red) and its history of expression (Green) are overlayed. No big differences are found between the two signals apart from small clones of current expression present in both control and mutant. *Δm1* hemizygous wing discs present a severe deformation of AP boundary and the P size is severely affected. Scalebars: 100μm

**Figure 2 – figure supplement 3: Vestigial expression in OR463 mutants.** In magenta, anti-Wg immunostaining, in green anti-Vg. **A.** Control (R2-WT/apDG3) L3 wing disc. Wg is detected in its stereotypic stripe along the wing pouch and is also detected in the hinge and notum. Vg is detected in the wing pouch and in the laterals of the proximal hinge. **B.** Hemizygous *Δm1* mutant (*R2-Δm1/apDG3*) L3 wing disc. Wg stripe is extended in the anterior compartment (arrow) coinciding with the outgrowth. Vg localizes throughout the outgrowth in a pattern highly reminiscent of the pouch staining, with its highest levels in along the DV boundary. **C.** Hemizygous Δm3 mutant (*R2-Δm3/apDG3*) L3 wing disc. Wg stripe is missing and only the outer Wg ring of the hinge is detected, the inner ring being reduce to a group of cells. Vg is not detected at levels comparable to the WT discs.

**Figure 2 – figure supplement 4. Model for the development of mirror image duplications in ap OR463 mutants. A.** Model of Wild type wing development across larval, pupal and adult stages. The AP boundary (green) intersect with the DV boundary (purple) in only one spot (asterisk) during larval stages. In pupal stages, the wing pouch everts along the DV boundary, that become the wing margin. As wing veins are patterned by the AP border, their location is relatively parallel to it. **A'.** Example of wild-type wing disc and wing extracted from figure 1 and 2. The morphology of the posterior border is highlighted. It consists of a single row of fine bristles and looks distinctively different from the double-row bristles near of the tip of the. Wing or the triple-row bristles at the anterior margin. B. Wing disc model in which the PD size is affected but still occupies part of the pouch. In these cases, the AP border intersect with the DV boundary in two points which are far enough to specify two independent pouches. The "secondary" pouch does not present a real intersection, but both AP and DV boundaries coincide for a stretch after meeting. During pupal stages, after wing disc eversion, the outgrowth will present a dorsal side with A identity and a ventral side with P identity, resulting in venation defects. These veins, moreover, will be patterned parallel to the margin, as Hh and Dpp will be expressed along the DV boundary. **B'.** Example of a *Δm1* wing disc and wing extracted from figure 1 and 2 that might be following this model. Note the presence of tip-margin bristles in the posterior outgrowth **C.** Wing disc in which PD is almost missing. In these cases, the whole P compartment will behave as does the outgrowth in panel B. **C'.** Example of a *Δm1*/*ap$^{DG3}$* wing disc and wing extracted from figure 1 and 2 that might be following this case. In this case, A-specific dorsal triple-row bristles can be detected at the posterior margin. **D.** Model of wing development in which the DV is totally missing. In these cases, DV and AP boundaries are no longer crossing each other. If in close proximity, as it is the case here, a small wing pouch will still be specified. During wing disc eversion, the DV boundary will only present A identity, P compartment being reduced to one of the two sides of the wing depending on the P size, it might form a small "bag-like" structure. **D'** Example of a *Δm1*/DG3 wing disc and wing extracted from figure 1 and 2 that might be following this model. Note that the margin of this wing is only composed of anterior and tip-specific margin bristles **E.** *Δm1* homozygous mutant wing and detail of the campaniform sensillae in the P wing.

**Figure 2 – figure supplement 5. Posterior hinge and Upd expression patterns are affected in *ap* mutants. A**. Locali-zation of Ptc (Magenta) and Hth (Gray) in control wing discs. Hth is expressed along the hinge. (Posterior dorsal hinge is indicated with an arrowhead) **A'.** Localization of Ptc and Hth in *Δm1*/*ap$^{DG3}$* mutants. In these cases, P hinge is depleted (arrowhead) and the Ptc stripe deviated. **B.** *UAS*-CD8:GFP driven by *upd-Gal4* in wild-type wing discs. In the control discs, GFP signal could be detected in three main spots in the dorsal hinge (arrowheads) and two weak areas of expression in the ventral body wall (asterisks). **B'.** *UAS*-CD8:GFP driven by *upd-Gal4* in *ΔOR463*/ *ap$^{DG3}$* hemizygous background. Notice that the P source of Upd in the hinge is totally lost in this condition. Scale bars: 100μm

**Figure 5 – figure supplement 1. Deletion analysis within m3 region. A.** Schematic representation of the different deletions and representative phenotypes. Examples of the loss of the GATA binding site and the most distal m3 region are shown. Note that *Δm3.*3 flies do not develop wing structures. **B.** Scoring of the penetrance of mutant phenotypes in the different deletions. **C.** anti-Ap and anti-Wg immunostaining in both *Δm3* deletion and *Δm3.3*. In both cases Ap localization is only residual within the anterior hinge.

**Figure 5 – figure supplement 2. Correct spacing between GATA and HOX binding sites is essential. A.** Adult wing phenotype of control flies. **B.** Loss of wing produced upon extension of the spacing between the GATA and HOX binding sites by 6pb Notice that this genotype never resulted in normal wings (See scoring of Figure 5D). Wings were either completely missing (35%) or showed sever phenotype. **C.** Example wing phenotype resulting from the contraction of the linker between the GATA and HOX binding sites. In this case, observed phenotypes were clearly weaker than for m3+6bp. Apart from normal wings (30%), most of the wings had an outgrowth from the posterior compartment or looked as depicted. **D.** Adult wing phenotype of control flies (Same specimen as in A). **E.** Loss of wing produced upon *Δm3* deletion (same as Figure 1G). **F.** Example of the wing phenotypes obtained upon contraction of the m2's GATA-HOX linking sequence in the absence of m3. Note that the majority (68%) of wings were missing for this genotype. Among the rest, most wings looked as shown in F'. A few cases as shown in F'' were also present.

**Figure 6 – figure supplement 1. Pattern of Grn:GFP localization during wing development.** *grn:*GFP wing disc stained with anti-Ap and anti-Wg. (56h) At this stage Grn:GFP localizes to the presumptive hinge and seems to be highly down- regulated in the future notum and incipient pouch (marked by Wg). Grn:GFP was detected at higher levels in the anterior compartment. It was also detected broadly in the peripodial membrane. (62h) Similar Grn:GFP localization to that of 56h. (78h) Grn:GFP localization is higher in the proximal hinge, but persist at low levels in some lateral areas. Peripodial expression is higher in the lateral sides. (94h) Grn:GFP localizes sharply in the proximal hinge, totally excluded from the notum. Proximal hinge levels are very low. Only the cubic cells of the peripodial membrane seem to express *grn*. Arrowheads indicate the intersection between trachea and the disc proper. Scalebars: 50μm

**Figure 7 – figure supplement 1. *Antp* is required for clone survival in early stages and does not affect *ap* expression at later stages. A.** Example of wing disc in which *Antp* MARCM clones were generated during embryonic stages (0-24h) (See materials and methods for full genotype). In this case, many clones could be retrieved in other tissues (data not shown), but never in the disc proper of the wing disc. Clones, marked by the presence of GFP, could only be retrieved in the peripodial membrane (detail of the peripodial membrane in the right panel). In magenta, anti-Ap immunostaining reveals normal Ap pattern (left panel). **B.** Example of a wing disc of the same genotype as in A in which the clones were generated at 48h in development. In this case, small *Antp* clones (GFP positive) could be detected in the disc proper. Anti-Ap immunostaining revealed no change in the levels inside the clone (arrowheads).

## Acknowledgements

We thank Dr. Carlos Estella and Dr. Minkyoung Lee for their comments on the manuscript. We thank Basil Willi for the construction of the plasmid used for generating allele $ap^{R2.\Delta m3.5}$ and to Prof. Kristen Guss, Prof. Isabel Guerrero and Dr. Natalia Azpiazu for the provided reagents. We are grateful to Karin Mauro, Bernadette Bruno, Gina Evora, Sermin Kösger and Maria del Consuelo Zuluaga Gomez for constant and reliable supply of the world's best fly food. The work in the laboratory of M.A. was supported by grants from the Swiss National Science Foundation (310030_192659/1) and by funds from the Kanton Basel-Stadt and Basel-Land. GA was supported by 'Fellowships for Excellence' from the International PhD Program in Molecular Life Sciences of the Biozentrum, University of Basel.

## References

Aldaz, S., Escudero, L. M., & Freeman, M. (2010). Live imaging of Drosophila imaginal disc development. *Proceedings of the National Academy of Sciences*, *107*(32), 14217–14222. https://doi.org/10.1073/pnas.1008623107

Arnold, P., Erb, I., Pachkov, M., Molina, N., & van Nimwegen, E. (2011). MotEvo: integrated Bayesian probabilistic methods for inferring regulatory sites and motifs on multiple alignments of DNA sequences. *Bioinformatics*, *28*(4), 487–494. https://doi.org/10.1093/bioinformatics/btr695

Baena-Lopez, L. A., & García-Bellido, A. (2006). Control of growth and positional information by the graded vestigial expression pattern in the wing of Drosophila melanogaster. *Proceedings of the National Academy of Sciences*, *103*(37), 13734–13739. https://doi.org/doi:10.1073/pnas.0606092103

Baonza, A., Roch, F., & Martín-Blanco, E. (2000). DER signaling restricts the boundaries of the wing field during Drosophila development. *Proceedings of the National Academy of Sciences*, *97*(13), 7331–7335. https://doi.org/10.1073/pnas.97.13.7331

Basler, K., & Struhl, G. (1994). Compartment boundaries and the control of Drosopfiffa limb pattern by hedgehog protein. *Nature*, *368*(6468), 208–214. https://doi.org/10.1038/368208a0

Bieli, D., Kanca, O., Gohl, D., Denes, A., Schedl, P., Affolter, M., & Müller, M. (2015). The Drosophila melanogaster Mutants apblot and apXasta Affect an Essential apterous Wing Enhancer. *G3 (Bethesda)*, *5*(6), 1129–1143. https://doi.org/10.1534/g3.115.017707

Bieli, D., Kanca, O., Requena, D., Hamaratoglu, F., Gohl, D., Schedl, P., Affolter, M., Slattery, M., Müller, M., & Estella, C. (2015). Establishment of a Developmental Compartment Requires Interactions between Three Synergistic Cis-regulatory Modules. *Plos Genetics*, *11*(10), e1005376. https://doi.org/10.1371/journal.pgen.1005376

Blair, S. S., Brower, D. L., Thomas, J. B., & Zavortink, M. (1994). The role of apterous in the control of dorsoventral compartmentalization and PS integrin gene expression in the developing wing of Drosophila. *Development*, *120*(7), 1805–1815. https://doi.org/10.1242/dev.120.7.1805

Brower, D. L. (1984). Posterior-to-anterior transformation in engrailed wing imaginal disks of Drosophila. *Nature*, *310*(5977), 496–497. https://doi.org/10.1038/310496a0

Brown, S., & Castelli-Gair Hombria, J. (2000). Drosophila grain encodes a GATA transcription factor required for cell rearrangement during morphogenesis. *Development*, *127*(22), 4867–4876. https://doi.org/10.1242/dev.127.22.4867

Bulajić, M., Srivastava, D., Dasen, J. S., Wichterle, H., Mahony, S., & Mazzoni, E. O. (2020). Differential abilities to engage inaccessible chromatin diversify vertebrate Hox binding patterns. *Development*, *147*(22). https://doi.org/10.1242/dev.194761

Bürglin, T. R., & Affolter, M. (2016). Homeodomain proteins: an update. *Chromosoma*, *125*(3), 497–521. https://doi.org/10.1007/s00412-015-0543-8

Capdevila, J., & Guerrero, I. (1994). TARGETED EXPRESSION OF THE SIGNALING MOLECULE DECAPENTAPLEGIC INDUCES PATTERN DUPLICATIONS AND GROWTH ALTERATIONS IN DROSOPHILA WINGS. *Embo Journal*, *13*(19), 4459–4468. https://doi.org/10.1002/j.1460-2075.1994.tb06768.x

Chen, M., Gao, E., Lin, G., Shen, J., & Wang, D. (2023). The transcription factor optomotor-blind restricts apterous expression through TrxG and PcG genes. *Dev Biol*, *497*, 59–67. https://doi.org/10.1016/j.ydbio.2023.03.002

Cohen, B., McGuffin, M. E., Pfeifle, C., Segal, D., & Cohen, S. M. (1992). apterous, a gene required for imaginal disc development in Drosophila encodes a member of the LIM family of developmental regulatory proteins. *Genes Dev*, *6*(5), 715–729. https://doi.org/10.1101/gad.6.5.715

Couso, J. P., Bate, M., & Martínez-Arias, A. (1993). A wingless-dependent polar coordinate system in Drosophila imaginal discs. *Science*, *259*(5094), 484–489. https://doi.org/10.1126/science.8424170

Couso, J. P., Knust, E., & Martinez Arias, A. (1995). Serrate and wingless cooperate to induce vestigial gene expression and wing formation in Drosophila. *Curr Biol*, *5*(12), 1437–1448. https://doi.org/10.1016/s0960-9822(95)00281-8

Dahmann, C., Oates, A. C., & Brand, M. (2011). Boundary formation and maintenance in tissue development. *Nature Reviews Genetics*, *12*(1), 43–55. https://doi.org/10.1038/nrg2902

Diaz-Benjumea, F. J., & Cohen, S. M. (1993). Interaction between dorsal and ventral cells in the imaginal disc directs wing development in Drosophila. *Cell*, *75*(4), 741–752. https://doi.org/10.1016/0092-8674(93)90494-b

Dinges, G. F., Chockley, A. S., Bockemühl, T., Ito, K., Blanke, A., & Büschges, A. (2021). Location and arrangement of campaniform sensilla in Drosophila melanogaster. *Journal of Comparative Neurology*, *529*(4), 905–925. https://doi.org/https://doi.org/10.1002/cne.24987

Evans, C. J., Olson, J. M., Ngo, K. T., Kim, E., Lee, N. E., Kuoy, E., Patananan, A. N., Sitz, D., Tran, P., Do, M.-T., Yackle, K., Cespedes, A., Hartenstein, V., Call, G. B., & Banerjee, U. (2009). G-TRACE: rapid Gal4-based cell lineage analysis in Drosophila. *Nature Methods*, *6*(8), 603–605. https://doi.org/10.1038/nmeth.1356

Everetts, N. J., Worley, M. I., Yasutomi, R., Yosef, N., & Hariharan, I. K. (2021). Single-cell transcriptomics of the Drosophila wing disc reveals instructive epithelium-to-myoblast interactions. *eLife*, *10*, e61276. https://doi.org/10.7554/eLife.61276

Fang, C., Xin, Y., Sun, T., Monteiro, A., Ye, Z., Dai, F., Lu, C., & Tong, X. (2021). The Hox gene Antennapedia regulates wing development through 20-hydroxyecdysone in insect. *bioRxiv*, 2021.2005.2026.445904. https://doi.org/10.1101/2021.05.26.445904

Fernández-Fúnez, P., Lu, C. H., Rincón-Limas, D. E., García-Bellido, A., & Botas, J. (1998). The relative expression amounts of apterous and its co-factor dLdb/Chip are critical for dorso-ventral compartmentalization in the Drosophila wing. *EMBO J*, *17*(23), 6846–6853. https://doi.org/10.1093/emboj/17.23.6846

Fristrom, D., & Fristrom, J. W. (1975). The mechanism of evagination of imaginal discs of Drosophila melanogaster: I. General considerations. *Developmental Biology*, *43*(1), 1–23. https://doi.org/https://doi.org/10.1016/0012-1606(75)90127-X

Fuqua, T., Jordan, J., van Breugel, M. E., Halavatyi, A., Tischer, C., Polidoro, P., Abe, N., Tsai, A., Mann, R. S., Stern, D. L., & Crocker, J. (2020). Dense and pleiotropic regulatory information in a developmental enhancer. *Nature*, *587*(7833), 235–239. https://doi.org/10.1038/s41586-020-2816-5

Garcia-Bellido, A., Ripoll, P., & Morata, G. (1973). Developmental compartmentalisation of the wing disk of Drosophila. *Nat New Biol*, *245*(147), 251–253. https://doi.org/10.1038/newbio245251a0

Garcia-Bellido, A., Ripoll, P., & Morata, G. (1976). Developmental compartmentalization in the dorsal mesothoracic disc of Drosophila. *Developmental Biology*, *48*(1), 132–147. https://doi.org/https://doi.org/10.1016/0012-1606(76)90052-X

Garcia-Garcia, M. J., Ramain, P., Simpson, P., & Modolell, J. (1999). Different contributions of pannier and wingless to the patterning of the dorsal mesothorax of Drosophila. *Development*, *126*(16), 3523–3532. https://doi.org/10.1242/dev.126.16.3523

Gebelein, B., McKay, D. J., & Mann, R. S. (2004). Direct integration of Hox and segmentation gene inputs during Drosophila development. *Nature*, *431*(7009), 653–659. https://doi.org/10.1038/nature02946

Gratz, S. J., Cummings, A. M., Nguyen, J. N., Hamm, D. C., Donohue, L. K., Harrison, M. M., Wildonger, J., & O'Connor-Giles, K. M. (2013). Genome Engineering of Drosophila with the CRISPR RNA-Guided Cas9 Nuclease. *Genetics*, *194*(4), 1029–1035. https://doi.org/10.1534/genetics.113.152710

Guha, A., Lin, L., & Kornberg, T. B. (2009). Regulation of Drosophila matrix metalloprotease Mmp2 is essential for wing imaginal disc:trachea association and air sac tubulogenesis. *Developmental Biology*, *335*(2), 317–326. https://doi.org/https://doi.org/10.1016/j.ydbio.2009.09.005

Guillén, I., Mullor, J. L., Capdevila, J., Sánchez-Herrero, E., Morata, G., & Guerrero, I. (1995). The function of engrailed and the specification of Drosophila wing pattern. *Development*, *121*(10), 3447–3456. https://doi.org/10.1242/dev.121.10.3447

Hidalgo, A. (1998). Growth and patterning from the engrailed interface. *Int J Dev Biol*, *42*(3), 317–324.

Irvine, K. D., & Rauskolb, C. (2001). Boundaries in Development: Formation and Function. *Annual Review of Cell and Developmental Biology*, *17*(1), 189–214. https://doi.org/10.1146/annurev.cellbio.17.1.189

Johnstone, K., Wells, R. E., Strutt, D., & Zeidler, M. P. (2013). Localised JAK/STAT Pathway Activation Is Required for Drosophila Wing Hinge Development. *Plos One*, *8*(5), e65076. https://doi.org/10.1371/journal.pone.0065076

Kent, W. J., Sugnet, C. W., Furey, T. S., Roskin, K. M., Pringle, T. H., Zahler, A. M., & Haussler, D. (2002). The human genome browser at UCSC. *Genome Res*, *12*(6), 996–1006. https://doi.org/10.1101/gr.229102

Kim, J., Johnson, K., Chen, H. J., Carroll, S., & Laughon, A. (1997). Drosophila Mad binds to DNA and directly mediates activation of vestigial by Decapentaplegic. *Nature*, *388*(6639), 304–308. https://doi.org/10.1038/40906

Kim, J., Sebring, A., Esch, J. J., Kraus, M. E., Vorwerk, K., Magee, J., & Carroll, S. B. (1996). Integration of positional signals and regulation of wing formation and identity by Drosophila vestigial gene. *Nature*, *382*(6587), 133–138. https://doi.org/10.1038/382133a0

Klein, T., Couso, J. P., & Martinez Arias, A. (1998). Wing development and specification of dorsal cell fates in the absence of apterous in Drosophila. *Current Biology*, *8*(7), 417–421. https://doi.org/https://doi.org/10.1016/S0960-9822(98)70162-9

Kudron, M. M., Victorsen, A., Gevirtzman, L., Hillier, L. W., Fisher, W. W., Vafeados, D., Kirkey, M., Hammonds, A. S., Gersch, J., Ammouri, H., Wall, M. L., Moran, J., Steffen, D., Szynkarek, M., Seabrook-Sturgis, S., Jameel, N., Kadaba, M., Patton, J., Terrell, R.,…Waterston, R. H. (2018). The ModERN Resource: Genome-Wide Binding Profiles for Hundreds of Drosophila and Caenorhabditis elegans Transcription Factors. *Genetics*, *208*(3), 937–949. https://doi.org/10.1534/genetics.117.300657

Kurata, S., Go, M. J., Artavanis-Tsakonas, S., & Gehring, W. J. (2000). Notch signaling and the determination of appendage identity. *Proceedings of the National Academy of Sciences*, *97*(5), 2117–2122. https://doi.org/doi:10.1073/pnas.040556497

Kvon, E. Z., Zhu, Y., Kelman, G., Novak, C. S., Plajzer-Frick, I., Kato, M., Garvin, T. H., Pham, Q., Harrington, A. N., Hunter, R. D., Godoy, J., Meky, E. M., Akiyama, J. A., Afzal, V., Tran, S., Escande, F., Gilbert-Dussardier, B., Jean-Marçais, N., Hudaiberdiev, S.,…Pennacchio, L. A. (2020). Comprehensive In Vivo Interrogation Reveals Phenotypic Impact of Human Enhancer Variants. *Cell*, *180*(6), 1262–1271.e1215. https://doi.org/10.1016/j.cell.2020.02.031

Labun, K., Montague, T. G., Krause, M., Torres Cleuren, Y. N., Tjeldnes, H., & Valen, E. (2019). CHOPCHOP v3: expanding the CRISPR web toolbox beyond genome editing. *Nucleic Acids Research*, *47*(W1), W171–W174. https://doi.org/10.1093/nar/gkz365

Levine, M., Hafen, E., Garber, R. L., & Gehring, W. J. (1983). Spatial distribution of Antennapedia transcripts during Drosophila development. *The EMBO Journal*, *2*(11), 2037–2046. https://doi.org/https://doi.org/10.1002/j.1460-2075.1983.tb01697.x

Lin, S., Ewen-Campen, B., Ni, X., Housden, B. E., & Perrimon, N. (2015). In Vivo Transcriptional Activation Using CRISPR/Cas9 in Drosophila. *Genetics*, *201*(2), 433–442. https://doi.org/10.1534/genetics.115.181065

Loker, R., Sanner, J. E., & Mann, R. S. (2021). Cell-type-specific Hox regulatory strategies orchestrate tissue identity. *Current Biology*, *31*(19), 4246–4255.e4244. https://doi.org/10.1016/j.cub.2021.07.030

Lopez-Rivera, F., Foster Rhoades, O. K., Vincent, B. J., Pym, E. C. G., Bragdon, M. D. J., Estrada, J., Depace, A. H., & Wunderlich, Z. (2020). A Mutation in the Drosophila melanogastereve Stripe 2 Minimal Enhancer Is Buffered by Flanking Sequences. *G3: Genes|Genomes|Genetics*, g3.401777.402020. https://doi.org/10.1534/g3.120.401777

Metz, C. W. (1914). An Apterous Drosophila and Its Genetic Behavior. *The American Naturalist*, *48*(575), 675–692.

Milán, M., & Cohen, S. M. (1999). Regulation of LIM homeodomain activity in vivo: a tetramer of dLDB and apterous confers activity and capacity for regulation by dLMO. *Mol Cell*, *4*(2), 267–273. https://doi.org/10.1016/s1097-2765(00)80374-3

Morata, G., & Lawrence, P. A. (1975). Control of compartment development by the engrailed gene in Drosophila. *Nature*, *255*(5510), 614–617. https://doi.org/10.1038/255614a0

Neumann, C. J., & Cohen, S. M. (1997). Long-range action of Wingless organizes the dorsal-ventral axis of the Drosophila wing. *Development*, *124*(4), 871–880.

Nienhaus, U., Aegerter-Wilmsen, T., & Aegerter, C. M. (2012). In-vivo imaging of the Drosophila wing imaginal disc over time: novel insights on growth and boundary formation. *Plos One*, *7*(10), e47594. https://doi.org/10.1371/journal.pone.0047594

Paul, L., Wang, S.-H., Manivannan, S. N., Bonanno, L., Lewis, S., Austin, C. L., & Simcox, A. (2013). Dpp-induced Egfr signaling triggers postembryonic wing development in Drosophila.

*Proceedings of the National Academy of Sciences*, *110*(13), 5058–5063. https://doi.org/10.1073/pnas.1217538110

Paul, R., Giraud, G., Domsch, K., Duffraisse, M., Marmigère, F., Khan, S., Vanderperre, S., Lohmann, I., Stoks, R., Shashidhara, L. S., & Merabet, S. (2021). Hox dosage contributes to flight appendage morphology in Drosophila. *Nature Communications*, *12*(1), 2892. https://doi.org/10.1038/s41467-021-23293-8

Pérez-Pinera, P., Menéndez-González, M., & Vega, J. A. (2006). *Deletion of DNA sequences of using a polymerase chain reaction based approach* [deletion, mutagenesis, polymerase chain reaction, plasmid].

Port, F., & Bullock, S. L. (2016). Augmenting CRISPR applications in Drosophila with tRNA-flanked sgRNAs. *Nature Methods*, *13*(10), 852–854. https://doi.org/10.1038/nmeth.3972

Prince, F. d. r., Katsuyama, T., Oshima, Y., Plaza, S., Resendez-Perez, D., Berry, M., Kurata, S., & Gehring, W. J. (2008). The YPWM motif links Antennapedia to the basal transcriptional machinery. *Development*, *135*(9), 1669–1679. https://doi.org/10.1242/dev.018028

Qi, Lei S., Larson, Matthew H., Gilbert, Luke A., Doudna, Jennifer A., Weissman, Jonathan S., Arkin, Adam P., & Lim, Wendell A. (2013). Repurposing CRISPR as an RNA-Guided Platform for Sequence-Specific Control of Gene Expression. *Cell*, *152*(5), 1173–1183. https://doi.org/10.1016/j.cell.2013.02.022

Ramain, P., Heitzler, P., Haenlin, M., & Simpson, P. (1993). pannier, a negative regulator of achaete and scute in Drosophila, encodes a zinc finger protein with homology to the vertebrate transcription factor GATA-1. *Development*, *119*(4), 1277–1291. https://doi.org/10.1242/dev.119.4.1277

Recasens-Alvarez, C., Ferreira, A., & Milán, M. (2017). JAK/STAT controls organ size and fate specification by regulating morphogen production and signalling. *Nature Communications*, *8*(1), 13815. https://doi.org/10.1038/ncomms13815

Requena, D., Álvarez, J. A., Gabilondo, H., Loker, R., Mann, R. S., & Estella, C. (2017). Origins and Specification of the Drosophila Wing. *Current Biology*, *27*(24), 3826–3836.e3825. https://doi.org/https://doi.org/10.1016/j.cub.2017.11.023

Shariati, S. A., Dominguez, A., Xie, S., Wernig, M., Qi, L. S., & Skotheim, J. M. (2019). Reversible Disruption of Specific Transcription Factor-DNA Interactions Using CRISPR/Cas9. *Molecular Cell*, *74*(3), 622–633.e624. https://doi.org/https://doi.org/10.1016/j.molcel.2019.04.011

Shimell, M. J., Simon, J., Bender, W., & O'Connor, M. B. (1994). Enhancer point mutation results in a homeotic transformation in Drosophila. *Science*, *264*(5161), 968–971. https://doi.org/10.1126/science.7909957

Siepel, A., Bejerano, G., Pedersen, J. S., Hinrichs, A. S., Hou, M., Rosenbloom, K., Clawson, H., Spieth, J., Hillier, L. W., Richards, S., Weinstock, G. M., Wilson, R. K., Gibbs, R. A., Kent, W. J., Miller, W., & Haussler, D. (2005). Evolutionarily conserved elements in vertebrate, insect, worm, and yeast genomes. *Genome Res*, *15*(8), 1034–1050. https://doi.org/10.1101/gr.3715005

Tabata, T., Schwartz, C., Gustavson, E., Ali, Z., & Kornberg, T. B. (1995). Creating a Drosophila wing de novo, the role of engrailed, and the compartment border hypothesis. *Development*, *121*(10), 3359–3369. https://doi.org/10.1242/dev.121.10.3359

Tripathi, B. K., & Irvine, K. D. (2022). The wing imaginal disc. *Genetics*, *220*(4), iyac020. https://doi.org/10.1093/genetics/iyac020

Uemura, T., Shiomi, K., Togashi, S., & Takeichi, M. (1993). Mutation of twins encoding a regulator of protein phosphatase 2A leads to pattern duplication in Drosophila imaginal discs. *Genes Dev*, *7*(3), 429–440. https://doi.org/10.1101/gad.7.3.429

van Meyel, D. J., O'Keefe, D. D., Jurata, L. W., Thor, S., Gill, G. N., & Thomas, J. B. (1999). Chip and apterous physically interact to form a functional complex during Drosophila development. *Mol Cell*, *4*(2), 259–265. https://doi.org/10.1016/s1097-2765(00)80373-1

Wang, H., La Russa, M., & Qi, L. S. (2016). CRISPR/Cas9 in Genome Editing and Beyond. In R. D. Kornberg (Ed.), *Annual Review of Biochemistry, Vol 85* (Vol. 85, pp. 227–264). https://doi.org/10.1146/annurev-biochem-060815-014607

Wang, S. H., Simcox, A., & Campbell, G. (2000). Dual role for Drosophila epidermal growth factor receptor signaling in early wing disc development. *Genes Dev*, *14*(18), 2271–2276. https://doi.org/10.1101/gad.827000

Whittle, J. R. (1979). Replacement of posterior by anterior structures in the Drosophila wing caused by the mutation apterous-blot. *J Embryol Exp Morphol*, *53*, 291–303.

Williams, J. A., Paddock, S. W., Vorwerk, K., & Carroll, S. B. (1994). Organization of wing formation and induction of a wing-patterning gene at the dorsal/ventral compartment boundary. *Nature*, *368*(6469), 299–305. https://doi.org/10.1038/368299a0

Wu, J., & Cohen, S. M. (2002). Repression of Teashirt marks the initiation of wing development. *Development*, *129*(10), 2411–2418. https://doi.org/10.1242/dev.129.10.2411

Zecca, M., Basler, K., & Struhl, G. (1996). Direct and long-range action of a wingless morphogen gradient. *Cell*, *87*(5), 833–844. https://doi.org/10.1016/s0092-8674(00)81991-1

Zecca, M., & Struhl, G. (2002). Subdivision of the Drosophila wing imaginal disc by EGFR-mediated signaling. *Development*, *129*(6), 1357–1368. https://doi.org/10.1242/dev.129.6.1357

Zecca, M., & Struhl, G. (2007a). Control of Drosophila wing growth by the vestigialquadrant enhancer. *Development*, *134*(16), 3011–3020. https://doi.org/10.1242/dev.006445

Zecca, M., & Struhl, G. (2007b). Recruitment of cells into the Drosophila wing primordium by a feed-forward circuit of vestigial autoregulation. *Development*, *134*(16), 3001–3010. https://doi.org/10.1242/dev.006411

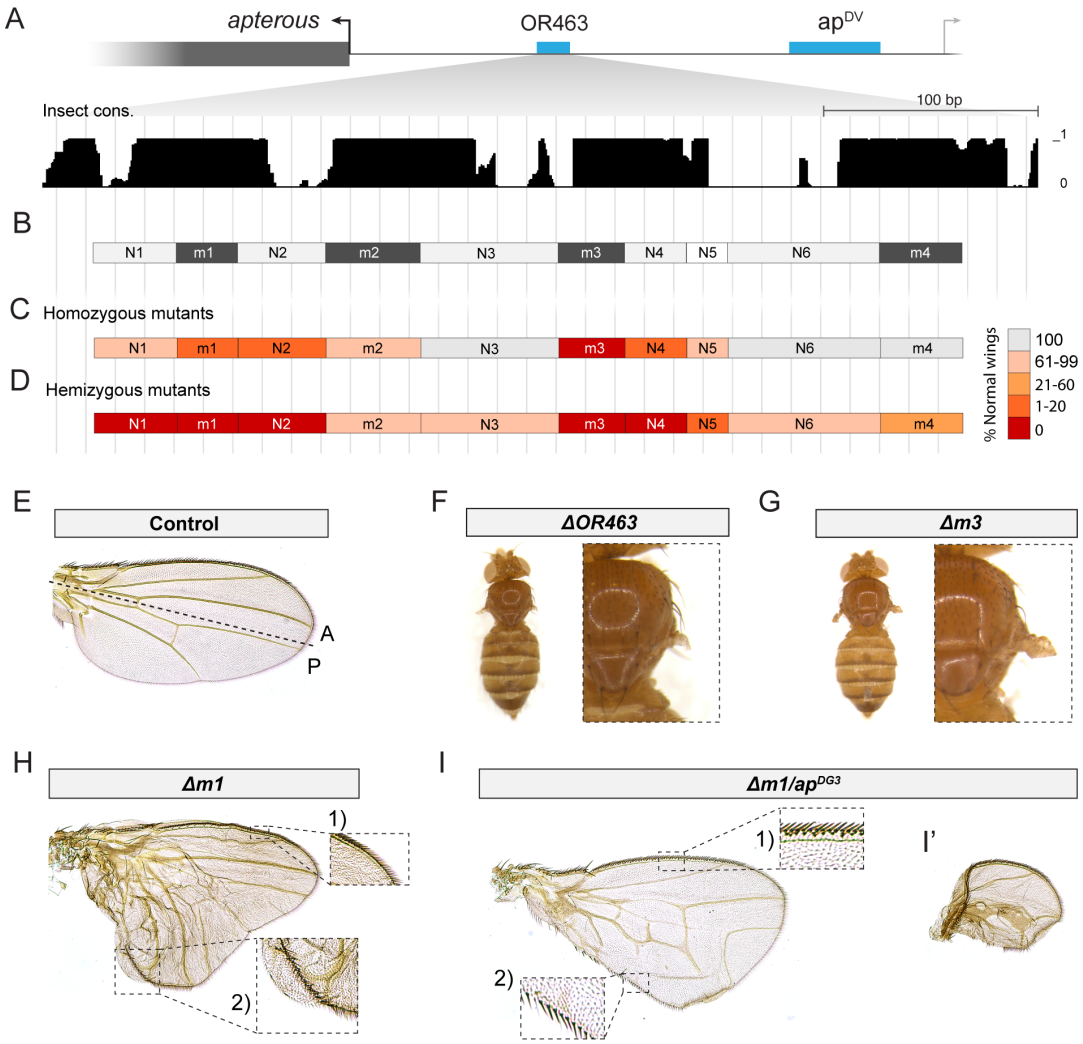


Figure 1

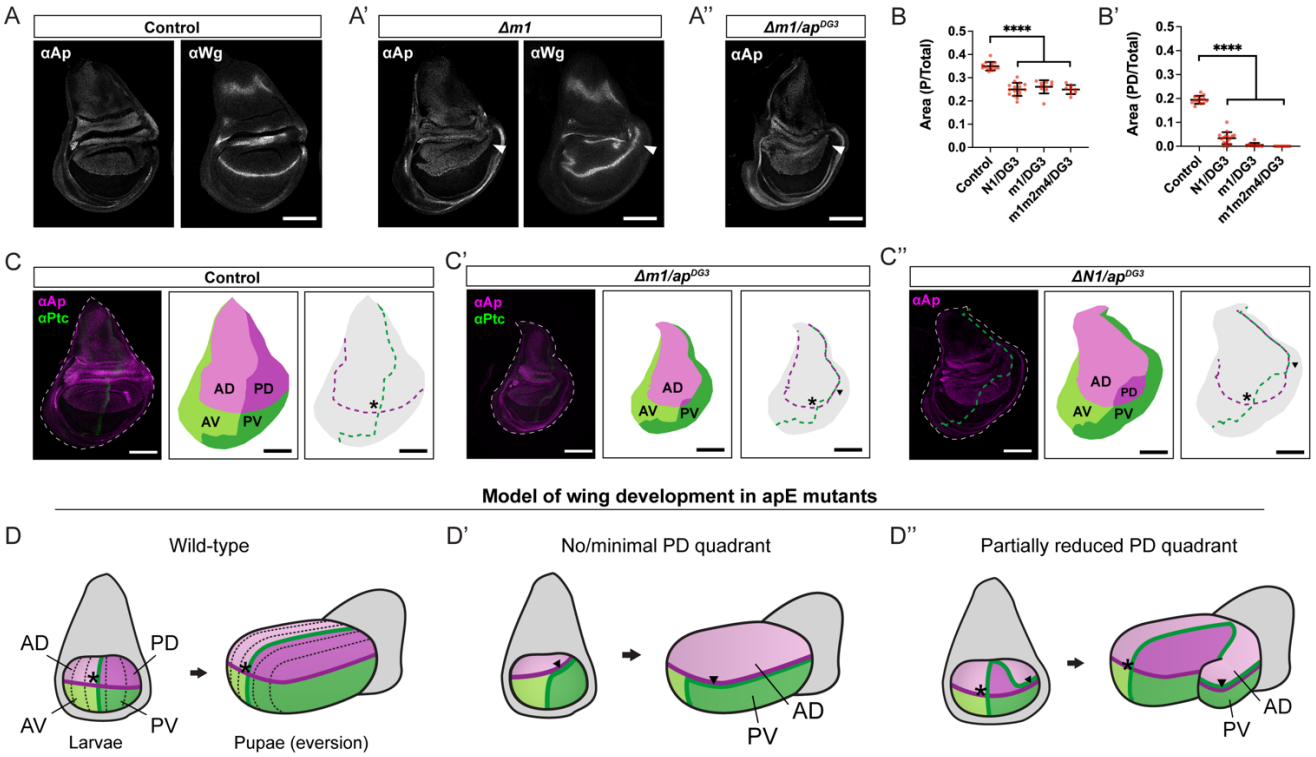


Figure 2

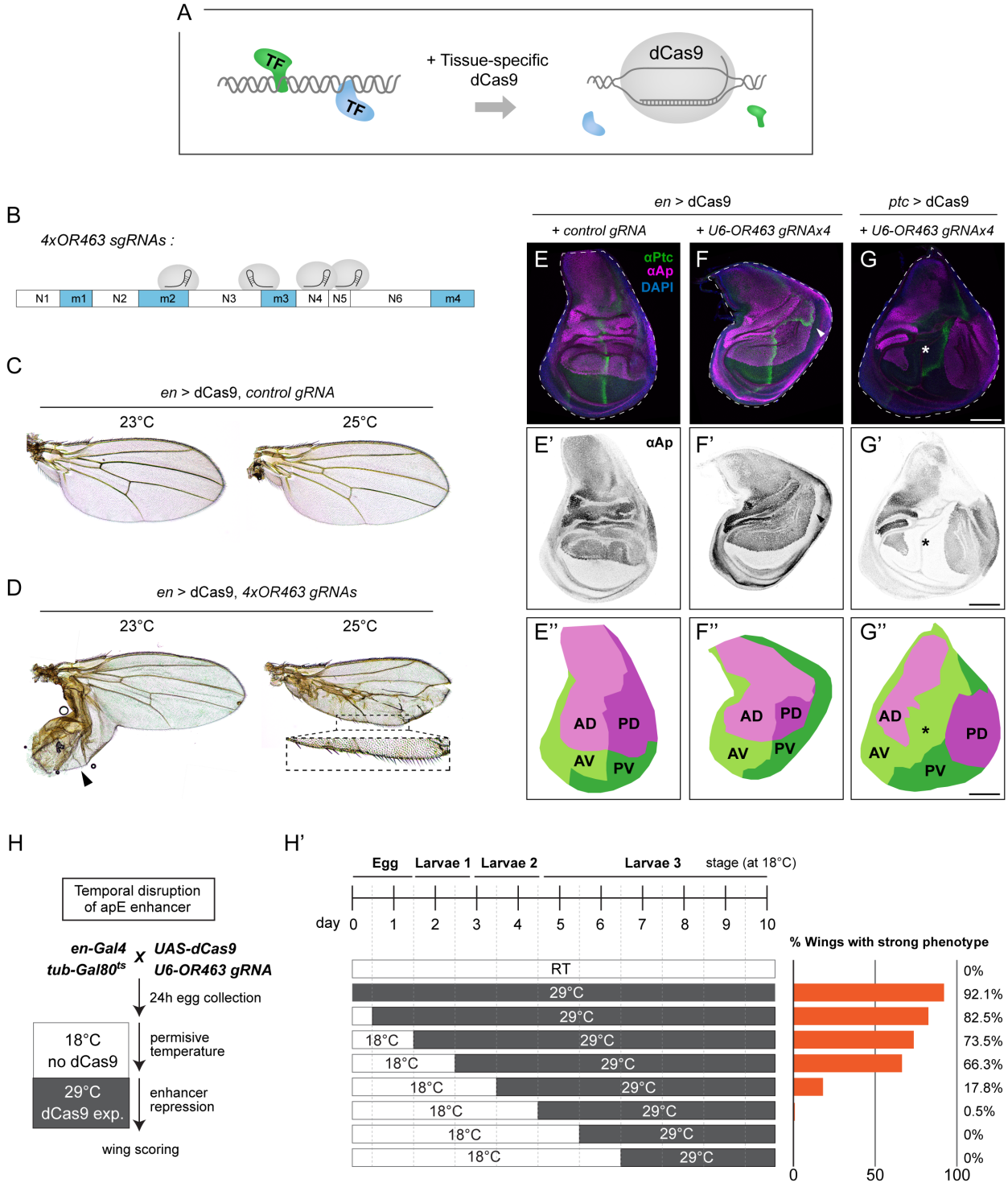


Figure 3

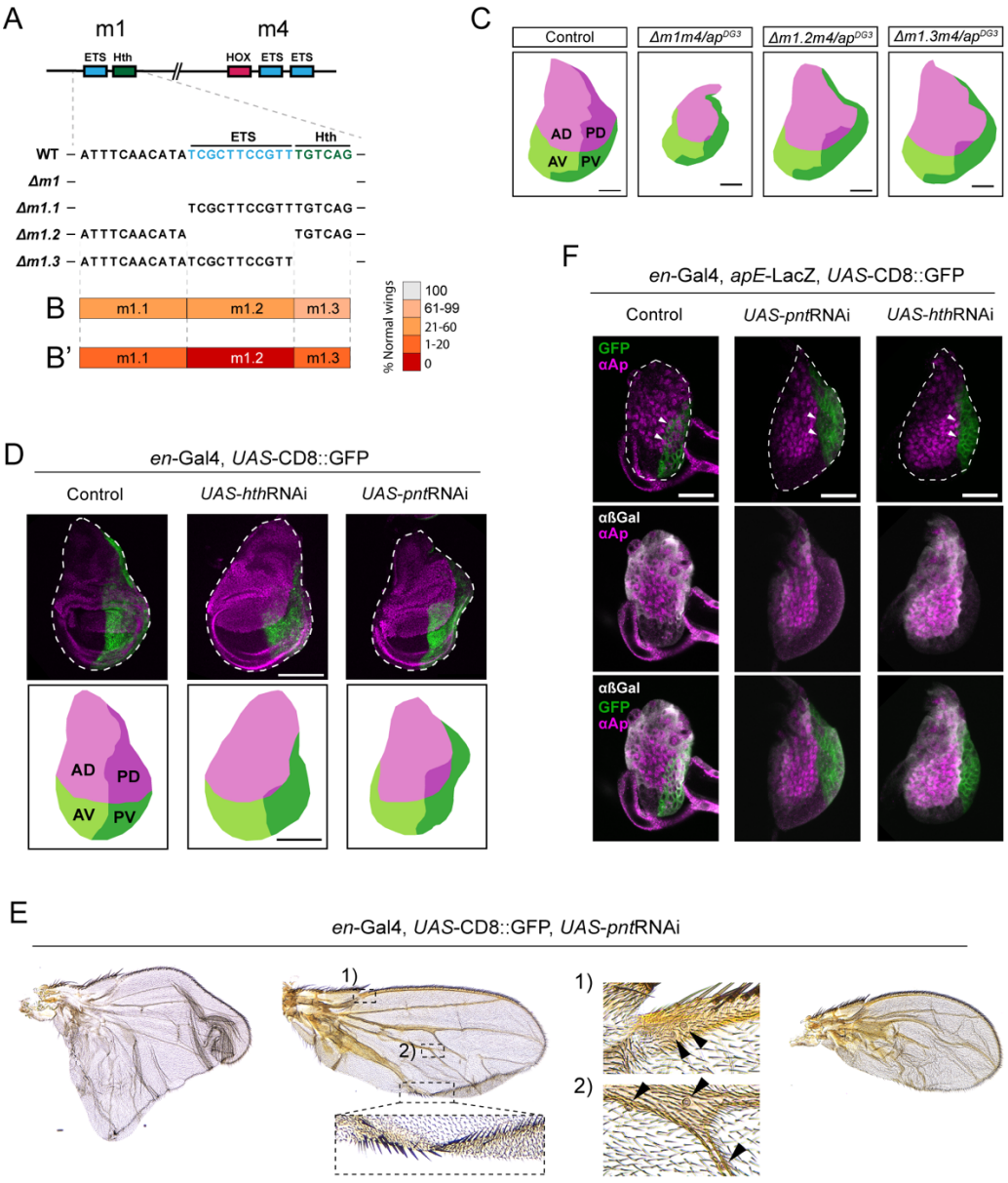


Figure 4

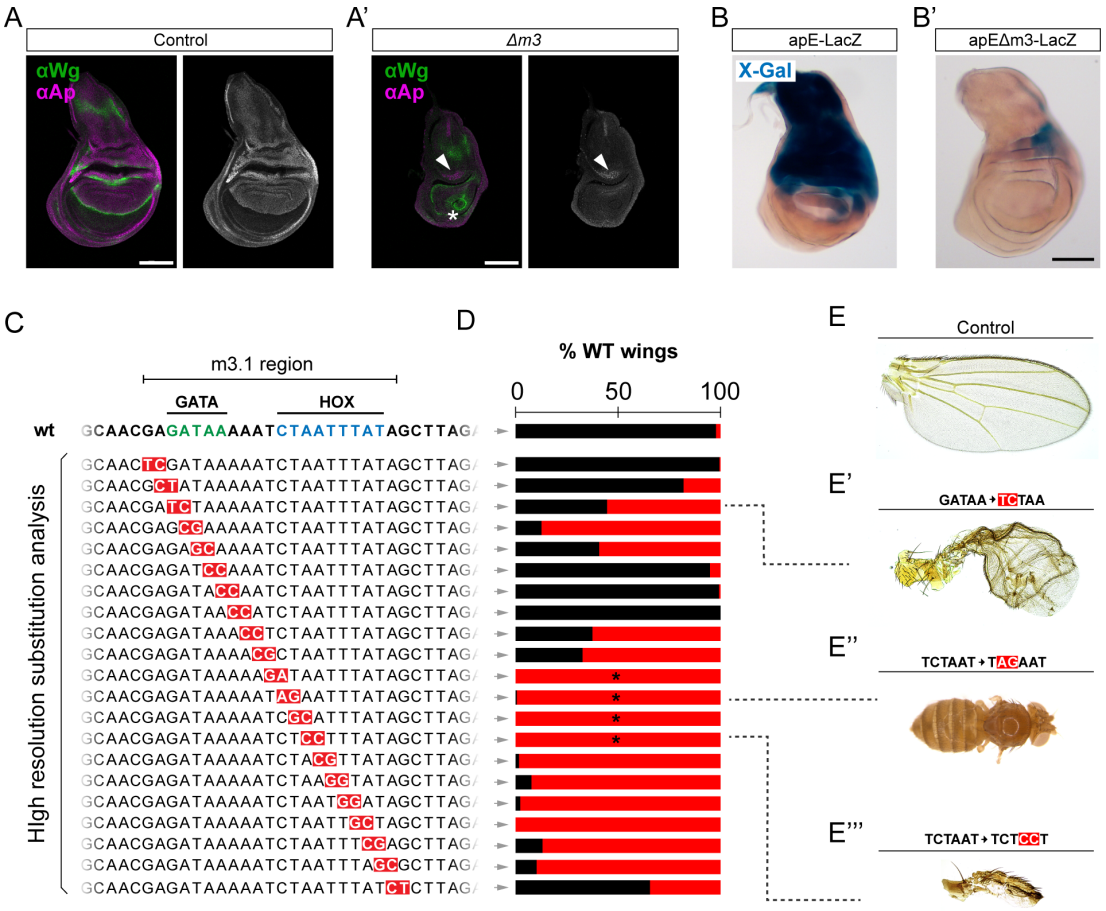


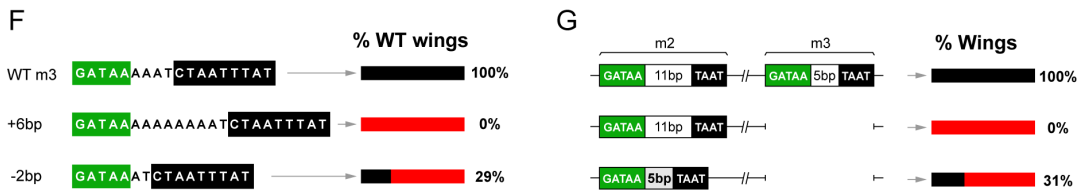


Figure 5

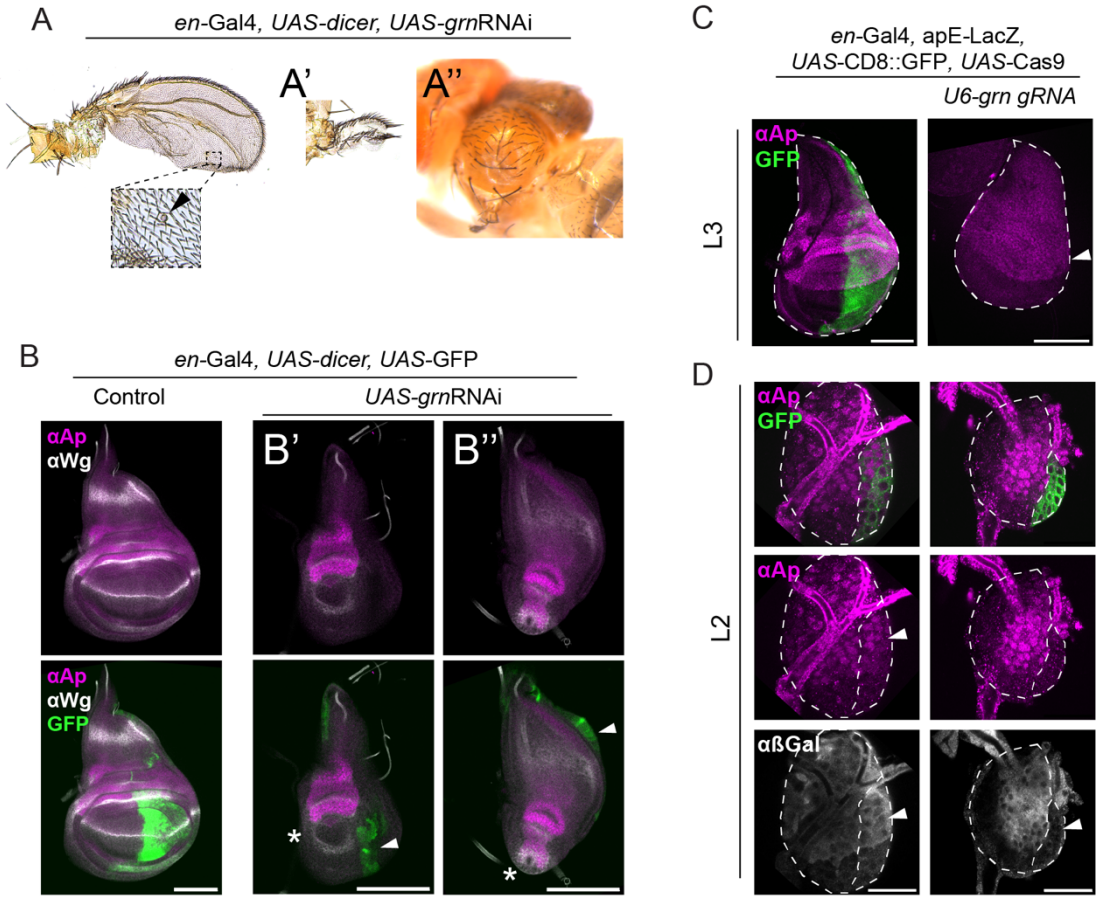


Figure 6

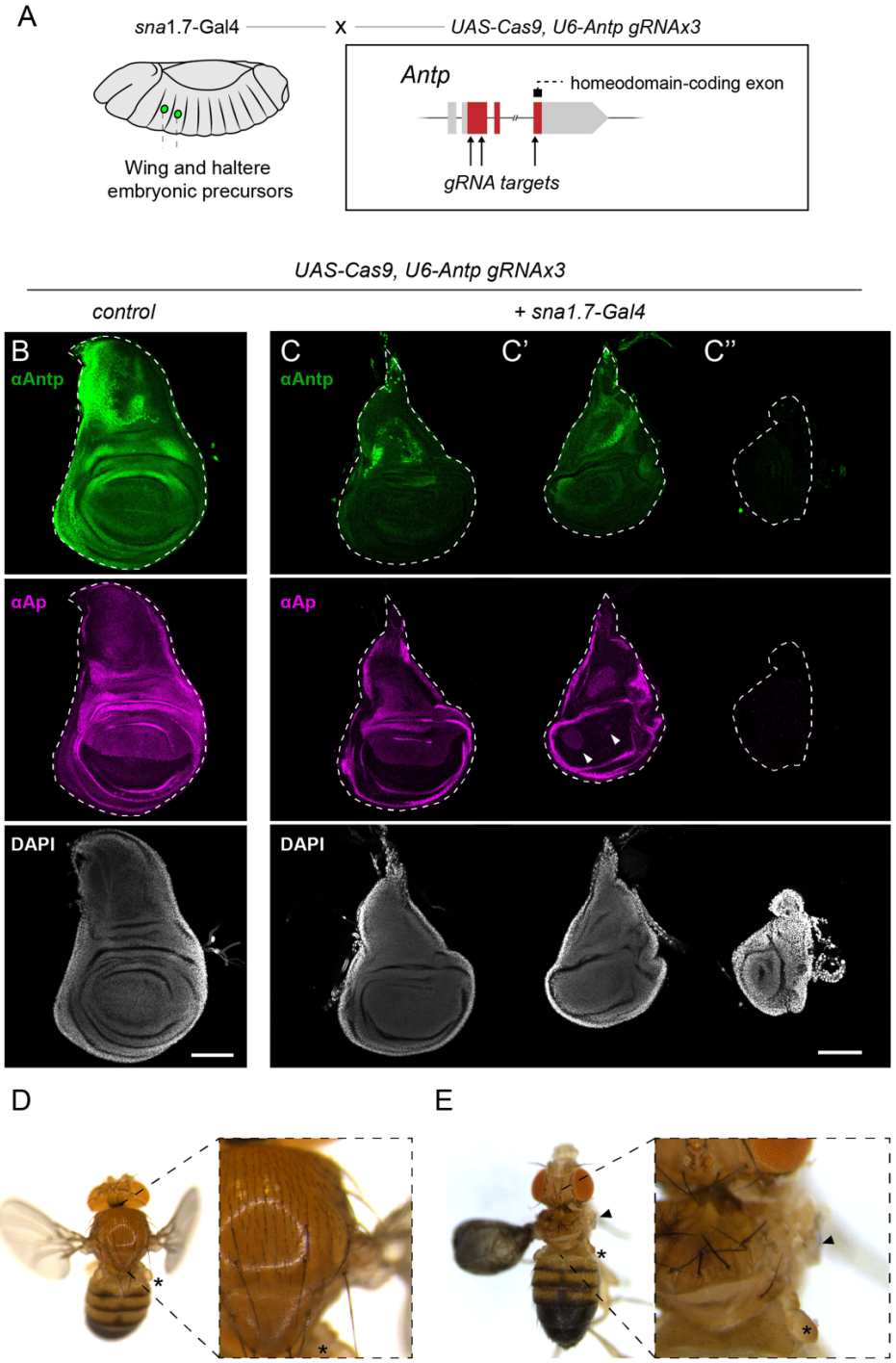


Figure 7

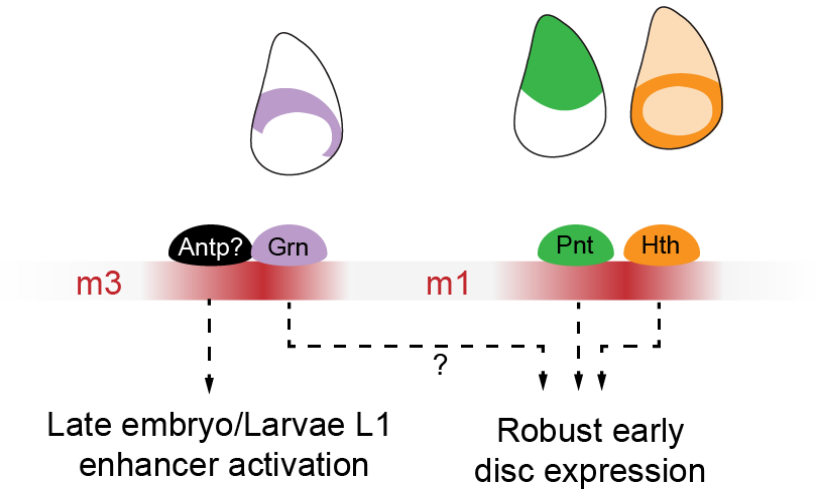


Figure 8